Joni Vehmas

Designing and Measuring a Novel Electromagnetic Transmission-Line Cloak for Microwave Frequencies

School of Electrical Engineering

Thesis submitted for examination for the degree of Master of Science in Technology.

Espoo 7.10.2011

Thesis supervisor:

Prof. Sergei Tretyakov

Thesis instructor:

D.Sc. (Tech.) Pekka Alitalo

Aalto University
School of Electrical Engineering

AALTO UNIVERSITY
SCHOOL OF ELECTRICAL ENGINEERING

ABSTRACT OF THE
MASTER'S THESIS

Author: Joni Vehmas

Title: Designing and Measuring
a Novel Electromagnetic Transmission-Line Cloak
for Microwave Frequencies

Date: 7.10.2011 Language: English Number of pages:8+70

Department of Radio Science and Technology

Professorship: Radio engineering Code: S-26

Supervisor: Prof. Sergei Tretyakov

Instructor: D.Sc. (Tech.) Pekka Alitalo

Transmission-line cloaking provides a simple yet wide-band solution for cloaking an object. The objective of this thesis is to design, manufacture and conduct free-space measurements in an anechoic chamber on a novel transmission-line cloak working at microwave frequencies. Special emphasis on the design is placed on ease of manufacture and practicality. It is shown both numerically and experimentally that the designed transmission-line cloak is capable of hiding a mesh-like metal object placed inside it from the incident wave in a variety of different scenarios and in a fairly wide bandwidth. Also, the agreement between simulations and measurements is good. Furthermore, the concept of using the cloak as an antenna at lower frequencies is introduced, and some preliminary proof-of-concept simulation results are shown.

Keywords: Cloaking, Transmission lines,
Antenna blockage

AALTO-YLIOPISTO
SÄHKÖTEKNIIKAN KORKEAKOULU

DIPLOMITYÖN
TIIVISTELMÄ

Tekijä: Joni Vehmas

Työn nimi: Uudenlaisen sähkömagneettisen mikroaaltoverhoamislaitteen suunnittelu ja mittaus

Päivämäärä: 7.10.2011 Kieli: Englanti Sivumäärä:8+70

Radiotieteen ja -tekniikan laitos

Professuuri: Radiotekniikka Koodi: S-26

Valvoja: Prof. Sergei Tretyakov

Ohjaaja: TkT Pekka Alitalo

Siirtojohtoverkkoja hyödyntävät "näkymättömyysviitat" tarjoavat suhteellisen yksinkertaisen mutta kuitenkin laajakaistaisen ratkaisun metalliobjektin verhoamiseksi sähkömagneettisilta aalloilta. Tämän diplomityön tavoitteena on suunnitella ja valmistaa uudenlainen siirtojohtoihin perustuva rakenne kappaleiden verhoamiseksi mikroaalloilta ja suorittaa vapaan tilan mittauksia rakenteella kaiuttomassa huoneessa. Painopisteinä suunnittelussa ovat rakenteen valmistamisen helppous ja käytännöllisyys. Työssä osoitetaan niin numeerisesti kuin myös kokeellisesti, että suunnitellun rakenteen avulla pystytään tehokkaasti piilottamaan verkkomainen metalliesine melko laajalla taajuuskaistalla useassa eri mittaustapauksessa. Simulaatio- ja mittaustulokset ovat hyvin yhteneväisiä. Työssä näytetään myös tietokonesimulaatioita hyödyntäen, miten kyseistä rakennetta voidaan muokata siten, että sitä voidaan käyttää samanaikaisesti myös antennina alhaisemmilla taajuuksilla.

Avainsanat: verhoaminen, siirtojohdot, antennin peittäminen

Preface

This master's thesis is based on the work done in Aalto University at the Department of Radio Science and Engineering in the Advanced Artificial Materials and Smart Structures research group led by Prof. Sergei Tretyakov in 2011. I would like to take this opportunity to extend my gratitude to the following people who have helped me during the thesis writing process and/or the whole of my studies:

I would like to thank my supervisor Prof. Sergei Tretyakov and my instructor Dr. Pekka Alitalo for continuing help and guidance not only during the duration of my thesis work but also during my whole work history in the Department of Radio Science and Engineering and the former Radio Laboratory reaching as far back as the summer of the first year of my studies in 2007.

I would also like to thank Eino Kahra for providing invaluable help in the construction of the cloak and the measurement setup, Viktor Sibakov for helping with the ordering of the required materials and all the other co-workers who provided guidance and useful comments during the writing process.

Finally, I want to thank my family and especially my parents who have supported and encouraged me admirably during the whole of my studies at TKK and Aalto University.

Otaniemi, October 4, 2011

Joni Vehmas

Contents

Symbols and abbreviations

Symbols

A	area
A, B, C, D	components of a transmission matrix
C	capacitance
c	the speed of light in vacuum $\approx 2.9979 \times 10^8$ [m/s]
D	directivity
D_E	directivity of a E-plane sectoral horn antenna
D_H	directivity of a H-plane sectoral horn antenna
D_p	directivity of a pyramidal horn antenna
d	period of a structure
E	electric field
E_d	directly transmitted electric field (amplitude)
E_i	incident electric field (amplitude)
E_r	reflected electric field (amplitude)
E_s	scattered electric field (amplitude)
e_r	radiation efficiency
f	frequency
f_r	resonance frequency
G	antenna gain; conductance
H	magnetic field
h	separation between the plates of a parallel plate capacitor
HP_E	E-plane half power beamwidth
HP_H	H-plane half power beamwidth
I	current
j	imaginary unit
J_i	incident power density
k	propagation constant, i.e., the wavenumber
k_0	free-space propagation constant, i.e., the free-space wavenumber
k_{TL}	propagation constant, i.e., the wavenumber, inside a transmission-line
k_x, k_y, k_z	components of the propagation constant k
L	inductance
n	integer
$\mathbf{P}$	polarization vector
$\hat{p}$	unit polarization vector
P_r	received power
R	reflectivity level; resistance
r_{ff}	far-field distance
r_{nf}	near-field distance
r, θ, φ	spherical position coordinates
S	power density
$S_{11}, S_{12}, S_{21}, S_{22}$	scattering parameters
U	radiation intensity

V	voltage
v_g	group velocity
v_p	phase velocity
x, y, z	Cartesian position coordinates
$\hat{x}, \hat{y}, \hat{z}$	Cartesian unit vectors
Y	admittance
Z	impedance
Z_0	characteristic impedance
Z_B	Bloch impedance
Z_L	load impedance
Z_{TL}	characteristic impedance of a transmission line
α	attenuation constant, i.e., the real part of the complex propagation constant γ
β	phase constant, i.e., the imaginary part of the complex propagation constant γ
γ	complex propagation constant
ϵ	permittivity
ϵ_0	vacuum permittivity $\approx 8.8542 \times 10^{-12}$ [F/m]
ϵ_r	relative permittivity
λ	wavelength
μ	permeability
ρ	reflection coefficient
σ	scattering cross section
σ_{2D}	scattering width
$\sigma_{\mathrm{2D,tot}}$	total scattering width
Ω	unit solid angle
ω	angular frequency

Abbreviations

AUT	antenna under test
HFSS	high frequency structure simulator
IEEE	Institute of Electrical and Electronics Engineers
MATLAB	matrix laboratory
PCB	printed circuit board
RF	radio frequency, approx. 3 kHz – 300 GHz
TE	transverse electric
TM	transverse magnetic
TEM	transverse electric and magnetic
TL	transmission line
VNA	vector network analyzer
VSWR	voltage standing wave ratio

1 Introduction

Electromagnetic cloaking has been a very trendy topic in electromagnetics research in recent years. Electromagnetic cloak is a structure designed for making a given object "invisible" to the electromagnetic radiation of a certain wavelength, i.e., "cloaking" it. Cloaking is typically based on the use of so-called metamaterials, or electromagnetic metamaterials to be more precise. Though various differing definitions for the term are given, typically metamaterials are defined as artificial materials consisting of or containing electrically small inclusions, e.g., metal rods having diameter much smaller than the wavelength, which cause the material to exhibit properties observed neither in the constituent materials nor in nature [1]. Because the inclusions are electrically small, i.e., small relative to the wavelength, the incident wave does not "see" single inclusions but the material as a whole with certain effective material parameters, similar to how a white area filled with small closely spaced black circles looks gray when viewed from a distance.

But how can these metamaterials be used to hide or "cloak" an object? Several different approaches to cloaking can be taken. Two of the most well-known ones are scattering cancellation cloaking and transformation-based cloaking. In scattering cancellation cloaking, the idea is to match the object to be cloaked to the background material thus eliminating scattering from the object and making the object invisible [2]. This is achieved typically by covering the object with a metamaterial cover with specific material properties. In transformation-based cloaking, on the other hand, the basic principle is that by pulling and stretching the original Cartesian coordinate mesh so that the fields no longer penetrate into a certain region of space at all, we can hide that part of space completely [3, 4]. In practice, this sort of deformation of space can effectively be, again, achieved with metamaterials with very specific material properties. However, the problem with both of these methods is that the metamaterials needed can be very difficult or even impossible to manufacture in practice.

Transmission-line-based cloaking provides a simpler alternative to the aforementioned cloaking methods [5]. In transmission-line-based cloaking the cloak consists of two parts: two- or three-dimensional transmission-line network and the so-called transition layer surrounding it. The wave incident on the cloak first hits the transition layer which guides, or couples, the wave to the transmission-line network. Then, the wave travels through the transmission-line network, with the transmission lines typically being parallel-strip lines. Finally, the wave is radiated out of the transmission-line network to free space, again, via the transition layer. The transition layer is typically realized by gradually enlarging the parallel-strip transmission lines and slightly bending them vertically. As the wave travels only inside the transmission lines, the volume between the lines is effectively cloaked. The obvious disadvantage of this cloaking method compared to the others mentioned is that the object to be cloaked has to fit inside the transmission-line network meaning that it cannot be very large electrically. On the other hand, transmission-line cloaks have much simpler structure and are much easier to manufacture and assemble compared to the scattering cancellation or transformation-based cloaks. Transmission-line

cloaks have also wide operational bandwidth.

The main objective of this thesis is to design, manufacture and conduct free-space measurements on a novel transmission-line cloak. The design is based on the earlier transmission-line cloak designs with several modifications made to the geometry of the cloak as well as tuning the cloak to work at our wanted operational frequency of 3 GHz. In the design, special emphasis is placed on the ease of manufacture, simplicity and practicality.

Though several measurements have been conducted on transmission-line cloaks in order to study their cloaking properties, all of these earlier measurements have been conducted inside a waveguide of some sort [6–8]. Most likely in a real-life application the cloak would not be placed inside a waveguide, but it would be used in free space. In this thesis, the first results for a free-space measurement of a transmission-line cloak are presented. To be precise, the cloaking properties of the designed transmission-line cloak are studied by measuring the radiation pattern of a horn antenna in an anechoic chamber in three cases: the antenna in free space, a metal object placed in front of the antenna in the near field, and a cloaked metal object placed in front of the antenna in the near field. By cloaking the metal object we should expect to restore the free space radiation pattern of the antenna. Several different measurement scenarios are employed where the position or the orientation of the cloak and the object is varied in relation to the antenna under test in order to determine the robustness of the cloaking effect.

In this work, the novel concept of using the transmission-line cloak as a radiating element, i.e., an antenna, is also briefly covered. Essentially, the transmission-line cloak can be transformed into a dipole-like antenna with a few simple modifications. This new structure still retains all the cloaking properties but can also work as an antenna at lower frequencies. This concept is explored using numerical simulations. Furthermore, it is demonstrated how the antenna resonance frequency of this new structure can be tuned by varying the capacitance of the structure. Lastly, it is shown how the cloak can also be transformed into a monopole-like antenna.

2 Electromagnetic cloaking

Electromagnetic cloaking, a subfield of metamaterials research, is a topic that has in recent years not only generated a wealth of interest among the metamaterial research community but also among the popular media and non-specialist press [9, 10]. Electromagnetic cloak is a structure designed for making a given object "invisible" to the electromagnetic radiation of a certain wavelength. It should be emphasized that cloaks can be and are designed for many different frequency bands, not just the optical frequencies, a fact sometimes ignored by the popular press. Several very different approaches can be taken for designing a cloaking structure. Three of the most popular cloaking techniques will be covered in this chapter with the more in-depth description of transmission-line cloaking reserved for Chapter 4. Also, the concepts of electromagnetic metamaterial and electromagnetic cloaking are discussed.

2.1 Electromagnetic metamaterials

Electromagnetic cloaking (or metamaterial cloaking) is a part of a larger field of research, metamaterials research. But what is a metamaterial? It turns out that there is no generally accepted definition. This is probably due to the relatively young age of the field as well as the multitude of different topics placed under the term "metamaterial". First of all, it should be noted that in this thesis the term "metamaterial" is used as a synonym for electromagnetic metamaterial omitting from the definition, e.g., acoustic and mechanical metamaterials. Still, even with this omittance we are left with a plethora of possible definitions. For example, "metamaterial" is defined by The Virtual Institute for Artificial Electromagnetic Materials and Metamaterials, Metamorphose VI AISBL as "an arrangement of artificial structural elements, designed to achieve advantageous and unusual electromagnetic properties" [11]. On the other hand, Caloz and Itoh define metamaterials as "artificial effectively homogeneous electromagnetic structures with unusual properties not readily available in nature" [12]. Despite of the varying and sometimes even somewhat conflicting definitions, two essential properties can be distinguished: metamaterials should exhibit properties observed neither in the constituent materials nor in nature [1]. The first of the two conditions means basically that by mixing several "natural" materials, we should get a new material, a metamaterial, that exhibits behavior that is not found in the materials that make up the metamaterial. The second condition demands that the unique properties of our new material should not only be unique compared to the constituent materials but also compared to all the materials found in nature. This is typically thought to exclude some very specific, rare and usually unstable conditions, e.g., plasma, where some "unnatural" or "exotic" behavior can be observed even in nature. That is why the term "not readily available" is used in the latter definition of a metamaterial. Another important distinction that is included in the latter definition is the effective homogeneity of the material. Essentially, this means that the metamaterial inclusions, i.e., the small parts comprising the material, have to be much smaller than the operational wavelength. When this is true,

the wave does not "see" a set of single inclusions but the material as a whole with effective material parameters. Though this is true to most metamaterials, as can be seen later, not to all.

2.2 Electromagnetic cloaking

Cloaking has been a popular subject in science fiction for several decades with some sort of cloaking device or invisibility cloak appearing in works as varied as Star Trek TV series and films, Predator films, and Harry Potter books. Though there have been several publications in the field of cloaking during the past 50 years, the concept of cloaking has remained steadily in the realm of science fiction – until recently. The new millennium has given rise to a newfound interest in cloaking, mainly thanks to a few key papers [2–4] that showed that maybe cloaking is not as far-fetched a concept as it had formerly seemed. The main approach in all of these papers was to use metamaterials to control the propagation of electromagnetic waves of a certain frequency, e.g., to make the waves go around the volume to be cloaked, thus rendering said volume "invisible" to the outside.

A distinction should be made between cloaking and stealth technology. In cloaking, the objective is to reduce the total scattering cross section of the object, i.e., minimize the scattering to all directions or ideally eliminate it altogether. On the other hand, in stealth technology the idea is typically to minimize the scattering only to a certain direction from where we expect the incident wave to arrive. This is typically achieved by using certain radar-absorbent materials and properly shaping the object.

2.3 Scattering cancellation cloaking

We say that we "see" an object when the light scattered from it hits our eye. Thus, if there is no scattering from the object, the object seems invisible to us. In scattering cancellation cloaking, the object is made "invisible" by "matching" it to the background material thus eliminating the scattering caused by the object. One of the key publications in this field was made by Alù and Engheta in 2005 [2]. The idea that they proposed was to cover a specific object with a material with certain material parameters ϵ_c and μ_c. Using fairly complex mathematics, it was shown that by choosing ϵ_c and μ_c as well as the thickness of the layer in a certain way, the scattering could be eliminated almost completely. In this initial paper the object was a dielectric sphere though the technique has later been suggested to work also with metal objects [13].

The physical principle behind the technique is that the polarization vector generated by the electric field inside the cover $\mathbf{P}_c = (\epsilon_c - \epsilon_0)\mathbf{E}$ cancels the polarization vector of the dielectric sphere $\mathbf{P} = (\epsilon - \epsilon_0)\mathbf{E}$, ϵ_c and ϵ being the permittivities of the cover and the object respectively and ϵ_0 being the vacuum permittivity [2]. This requires the polarization vectors to be antiparallel thus setting a condition $\epsilon_c < \epsilon_0$ which in practice means that the cover should be made of a metamaterial in order to achieve the cloaking effect. There are some materials readily available in na-

ture which have such low permittivity, but they are typically quite lossy and the material properties vary significantly with frequency. Furthermore, such low permittivity cannot be achieved for all frequencies using natural materials. It should also be noted that higher-order modes may also be excited in the cover and the object, but here it was assumed that the dipolar mode is dominant. This, however, is often the case especially when the object to be cloaked is electrically small, i.e., small compared to the wavelength.

An example design of a practical scattering cancellation cloak was presented in [14]. The cover material in this cloak design consists of metallic parallel-plate implants embedded in a dielectric region with positive relative permittivity. The parallel plate implants are placed radially around the dielectric cylinder to be cloaked as shown in Figure 1. At the design frequency of 100 THz, the real part of the permittivity of this material is negative enabling it to cancel out the dipolar radiation from the dielectric cylinder. In fact, pure noble metals also have this property. However, with pure noble metals the magnitude of the permittivity is several orders of magnitude larger than the permittivity of vacuum at frequencies below the visible range meaning that the dipolar radiation from the dielectric cylinder cannot be effectively canceled. Therefore, a composite material, like the one described before, is needed.

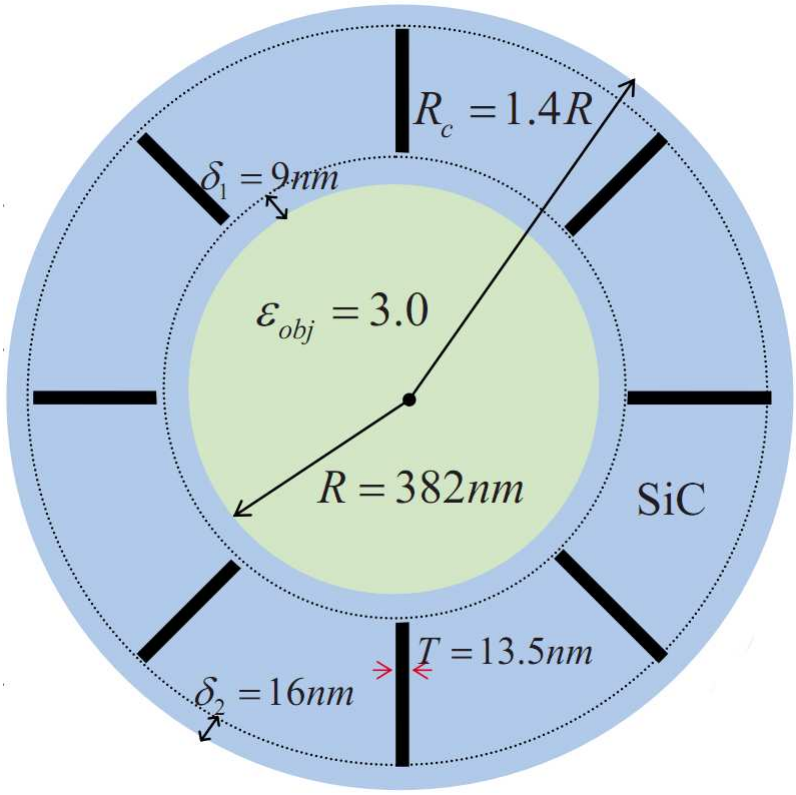

Figure 1: A practical scattering cancellation cloak designed for 100 THz (The different parts of the cloak are not drawn to scale) [14].

Though scattering cancellation techniques provide a fairly simple design and structure for the cloak, there are also several disadvantages. Firstly, this method works predominantly only for objects smaller than the operational wavelength with the cloak working best, i.e., providing quasi-perfect cloaking, with objects several decades smaller than the wavelength. With larger objects, the higher-order modes of the object are excited and canceling just the basic dipolar mode is not enough. It has been suggested that this problem can be overcome by using several cover layers [15] or by subdividing the large object into electrically smaller subunits, if possible, and then cloaking each of them individually [16]. Secondly, the scattering is shape-dependent, therefore we would need a separate cloak design for each object shape. Although design techniques have been developed for arbitrarily complex shapes [17], this does naturally make the design less versatile. Lastly, though the idea works in theory, manufacturing a metamaterial with the needed permittivity and permeability values or finding a suitable natural material could prove in practice to be very difficult or even impossible.

2.4 Transformation-based cloaking

Another approach to cloaking was introduced by Leonhardt [3] and Pendry et al. [4] independently in 2006. The main idea behind both of the papers is that by using a coordinate transformation we can pull and stretch the original Cartesian coordinate mesh in such a way that the fields no longer penetrate into a certain part of the space at all, e.g., by mapping a point in the electromagnetic space onto a sphere in the physical space. This idea is also illustrated in Figure 2. By plugging this transformation into Maxwell's equations, we can derive equations for the permittivity and permeability corresponding to this particular transform. For example for a cylindrical cloak, the permittivity and permeability tensors can be explicitly derived as [18]

$$\begin{aligned} \epsilon_r = \mu_r = \frac{r-a}{r}\epsilon_0 = \mu_\theta = \frac{r}{r-a} \\ \epsilon_z = \mu_z = \left(\frac{b}{b-a}\right)^2 \frac{r-a}{r}, \end{aligned} \tag{1}$$

where b and a are the radii of the cover and the cloaked cylindrical volume, respectively, and r is the radial coordinate. In order to realize such exotic material parameters, lossless anisotropic metamaterials are needed.

First realization of a coordinate transformation cloak was presented in [18]. This cylindrical cloak designed to work at microwaves is a two-dimensional simplification of the general case and works only with TE-polarized waves, i.e., waves with the E-field parallel to the axis of the cloak. The cloak consists of radially placed planar resonant particles with their shape varying with radial distance as shown in Figure 3. The design utilizes a simplified version of (1) which relies on linear variations of the inhomogeneity profile instead of parabolic variations [18]. This behavior can also be observed from Figure 3: The radial permeability of the cover material increases linearly as the radial distance increases while the other material parameter

components are constant.

The first experimental demonstration of optical cloaking was also achieved using transformation-based techniques [19]. The cloak used was a so-called carpet cloak introduced in [20]. In carpet cloaking, the cloaked object is "crushed" to a sheet using a coordinate transform. However, in the process the object becomes infinitely conducting meaning that in order to achieve any cloaking effect the object has to be placed on a conductive surface, the eponymous "carpet". Despite of this limitation this cloaking method has the advantage of nonsingular and isotropic material parameters. In [19], this technique was used to transform a mirror with a bump into a virtually flat mirror. This idea was further developed in [21] where a metal wedge of several centimeters was cloaked from optical wavelengths using a transformation-based cloak made of calcite, i.e., no metamaterials were used.

The main advantage of transformation-based cloaking compared to scattering cancellation techniques is that an object of any size can be cloaked as opposed to just objects smaller than the wavelength. Also, the geometry of the object does not affect the design of the cloak because the fields do not penetrate the cloaked volume at all. However as can be seen from (1), the conditions given for the permittivity and permeability are very specific and thus very hard to implement in practice even compared to the scattering cancellation cloaks. Furthermore, though metamaterials with such specific permittivity and permeability tensors are possible, they are most likely strongly dispersive and lossy and have the desired material parameter values only in a very narrow bandwidth. Therefore, simplified design equations have to be used in practical cloak designs like in the example above. These simplified design equations often provide a cloak that is easier to implement, but which provides imperfect cloaking capabilities.

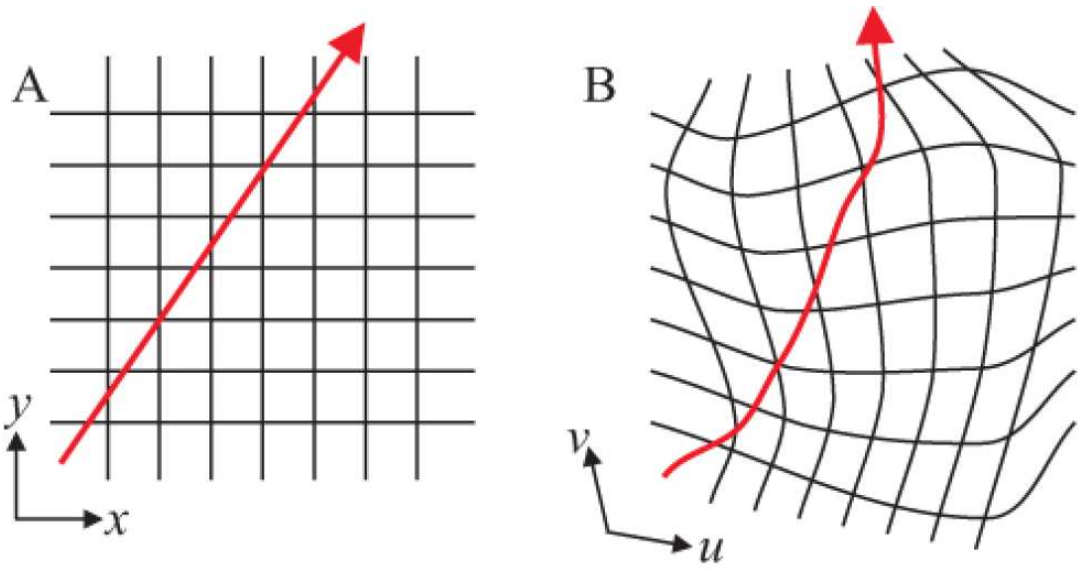

Figure 2: Principle behind coordinate transformation cloaking: (a) original space; (b) transformed space [4].

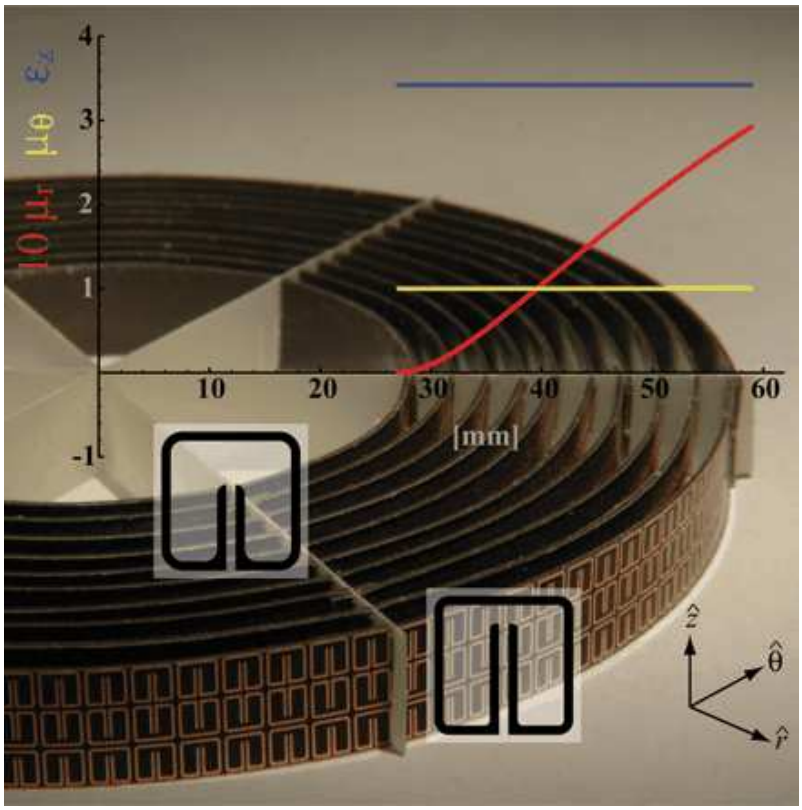

Figure 3: A practical transformation-based cloak [18].

2.5 Cloaking based on anomalous localized resonances

Another, very exotic, cloaking technique was introduced by Milton et al. also in 2006 [22]. Here, the cloaking is achieved by utilizing the so-called localized anomalous resonances. According to [22], an inhomogeneous body with piecewise constant moduli of material parameters exhibits anomalous resonance if, as the loss goes to zero, the field magnitude diverges throughout a specific region but converges to a smooth field outside that region. A cylindrical "superlens"', i.e., a lens which uses metamaterials to go beyond the diffraction limit, consisting of a coated cylinder with a core relative permittivity $\epsilon_c = 1$ and a shell relative permittivity $\epsilon_s = -1$, shown in Figure 4, is an example of such a body. It was shown in [22] and [23] that due to the anomalous resonances such a superlens can not only cloak itself from outside fields but also any objects close to it. This volume is denoted in Figure 4 by the dashed line. However, it should be noted that because this technique relies on strong resonances, it is very sensitive to frequency and other design variations as well as losses. A simulation example of cloaking using anomalous resonances is shown in Figure 5 where the cylindrical cloak described earlier is used for hiding a cluster of 7 polarizable dipoles in a hexagonal pattern from the incident electric field. The cloaking region is illustrated with a dashed line.

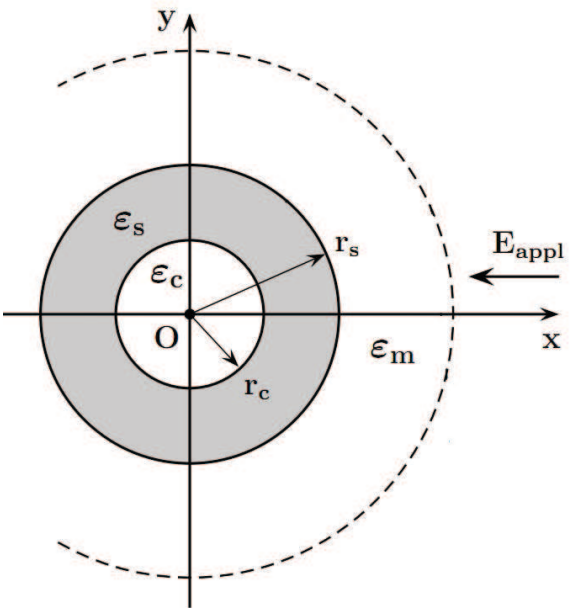

Figure 4: An example design of a cylindrical cloak employing anomalous resonances (the cloaking region is denoted by the dashed line) [23](mod.).

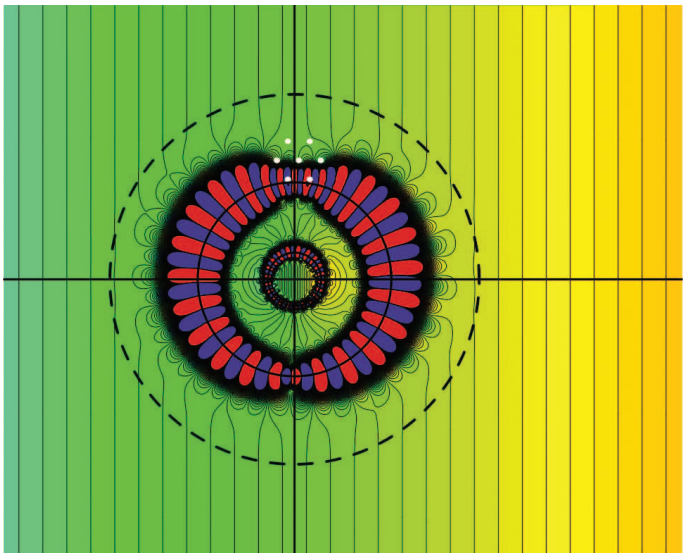

Figure 5: Potential distribution showing cloaking of a cluster of 7 polarizable dipoles in a hexagonal pattern [23].

3 Background

3.1 Scattering parameters

For low frequency circuits, the port voltages and currents can be easily defined unambiguously as the dimensions of the circuit are much smaller than the wavelength. However, the same does not necessarily hold true for higher frequencies, e.g., microwave frequencies 0.3 GHz – 300 GHz. In fact, only for TEM-waveguides, with the electric and magnetic fields perpendicular to the radiation direction, they can be defined unambiguously. For example, for a very common waveguide type, the rectangular waveguide, this can not be done. Even if we can define the voltages and currents unambiguously, measuring these voltages and currents in practice is quite problematic as we have to deal with the magnitude and phase of a wave traveling in a certain direction or of a standing wave. Thus, in microwave frequencies we can no longer just deal with voltages and currents, but we have to revert in our analysis back to electric and magnetic fields and propagating power. However, it would be useful if we could somehow analyze microwave circuits using just voltages, currents, and impedances as we could then employ circuit theory in our analysis. One way to achieve this is to use the scattering matrix. The scattering matrix which consist of scattering parameters or S-parameters relates the voltage waves incident on the ports of an N-port network to those reflected from the ports. These scattering parameters can be directly measured using a vector network analyzer (VNA). The scattering matrix is defined using this concept of incident and reflected voltage waves by [24]

$$\begin{bmatrix} V_1^- \\ V_2^- \\ \vdots \\ V_N^- \end{bmatrix} = \begin{bmatrix} S_{11} & S_{12} & \cdots & S_{1N} \\ S_{21} & & & \vdots \\ \vdots & & & \\ S_{N1} & \cdots & & S_{NN} \end{bmatrix} \begin{bmatrix} V_1^+ \\ V_2^+ \\ \vdots \\ V_N^+ \end{bmatrix}, \tag{2}$$

where coefficients S_{nm}, n and m being integers with $n, m \leq N$, are the scattering parameters or the S-parameters of the N-port. The matrix that these elements form is the scattering matrix or the S-matrix. A single element of the matrix is, thus, defined as

$$S_{nm} = \frac{V_n^-}{V_m^+}\Big|_{V_k^+ = 0 \text{ for } k \neq m}. \tag{3}$$

Parameter S_{nn} of any port n is called the reflection coefficient of the port. It tells how much of the power fed to port n is reflected back to that port when all the other ports are terminated in matched loads, i.e., there are no reflections from the other ports. Similarly, S_{nm} between any two ports n and m is called the transmission coefficient, and it tells how much of the power fed into port m is transmitted to port n when all the other ports are terminated in matched loads. [24, 25]

3.2 Transmission-line theory

Transmission-line theory, or TL-theory for short, can be considered both an extension of the basic circuit theory and a specialization of Maxwell's equations. The key difference between circuit theory and transmission-line theory is the electrical size of the network. In circuit theory, it is assumed that the physical dimensions of the network are very small compared to the wavelength whereas in transmission-line theory the length of transmission lines is typically of the same order as the wavelength. Because of this, the impedance and admittance of the line itself are significant and have to be taken into account. Therefore, we can no longer deal with just lumped elements but with distributed elements, i.e., with resistances per unit length instead of just resistances. In this part, the equations governing the propagation on a transmission line, the telegrapher's equations, are introduced, and the basic theory of periodic transmission lines is covered.

3.2.1 Telegrapher's equations

In transmission-line theory, conductors are usually presented as two-wire lines consisting of an infinite series of two-port elementary components each representing an infinitesimally small segment of the line. The considerable electric length of the transmission line causes series inductance, and there is capacitance between the two closely positioned conductors. Also, both the conductor losses (a series resistance) and the dielectric losses (a parallel conductance) have to be taken into account. Figure 6 shows a typical presentation of one such section of a transmission line with the length Δz. In Figure 6 and generally when speaking of transmission lines, the circuit parameters R, L, G, and C are given as ohms, henrys, siemens, or farads per unit length, respectively. The voltage and current of the line can be solved from the so-called telegrapher's equations [26]

$$\frac{\partial V(z,t)}{\partial z} = -RI(z,t) - L\frac{\partial I(z,t)}{\partial t} \tag{4}$$

$$\frac{\partial I(z,t)}{\partial z} = -GV(z,t) - C\frac{\partial V(z,t)}{\partial t}. \tag{5}$$

For sinusoidal signals (time-dependence of the complex signal $e^{j\omega t}$), (4) and (5) further reduce to

$$\frac{\partial V(z,t)}{\partial z} - \gamma^2 V(z) = 0 \tag{6}$$

$$\frac{\partial I(z,t)}{\partial z} - \gamma^2 I(z) = 0, \tag{7}$$

where γ is the complex propagation constant defined as

$$\gamma = \sqrt{(R + j\omega L)(G + j\omega C)} = \alpha + j\beta, \tag{8}$$

where α is the attenuation constant, and β is the phase constant.

Finally, the general solution for (6) and (7) is of the form

$$V(z) = V^+ e^{-\gamma z} + V^- e^{+\gamma z} \tag{9}$$

$$I(z) = \frac{V^+}{Z_0} e^{-\gamma z} - \frac{V^-}{Z_0} e^{+\gamma z} = I^+ e^{-\gamma z} + I^- e^{+\gamma z}, \tag{10}$$

where Z_0 is the characteristic impedance of the line given by

$$Z_0 = \sqrt{\frac{R + j\omega L}{G + j\omega C}}. \tag{11}$$

The values of R, G, L, and C depend on the transmission-line geometry.

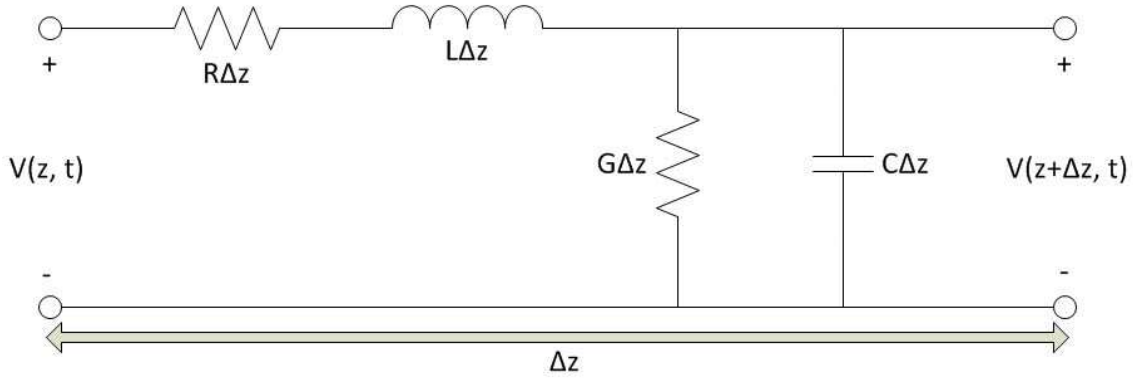

Figure 6: Equivalent circuit of a small transmission-line segment.

3.2.2 Periodic transmission-line structures

The analysis of periodic transmission-line structures (or in fact any periodic structure) is based on the Floquet theorem. The Floquet theorem applied to the electromagnetic wave propagation states that if a function $\mathbf{E}(x, y, z)$ satisfies the wave equation of a wave propagating along the z-direction in a periodic structure, then the function $\mathbf{E}(x, y, z + nd)$, where d is the period of the structure and n any integer number, can be represented as

$$\mathbf{E}(x, y, z + nd) = \mathbf{E}(x, y, z) e^{-\gamma nd}, \tag{12}$$

where γ is the complex propagation constant. Naturally the same principle applies also to the magnetic field [27].

Another way to analyze periodic structures is to use the so-called ABCD matrix [28–30]. Let us consider a line consisting of a cascade of m identical two-port networks. The voltages and currents on either side of the nth unit cell can be expressed as

$$\begin{bmatrix} V_n \\ I_n \end{bmatrix} = \begin{bmatrix} A & B \\ C & D \end{bmatrix} \begin{bmatrix} V_{n+1} \\ I_{n+1} \end{bmatrix}, \tag{13}$$

where A, B, C, and D depend on the constitution of the unit cell. For example, for a two-port consisting of a single series impedance Z, we get $A = D = 1$, $B = Z$, and $C = 0$. The convenience of the ABCD matrices comes from the fact that the total ABCD matrix of a cascade is found simply by multiplying the ABCD matrices of the individual two-ports. Thus, the matrix equation for the cascade of m identical two-port networks can be written as

$$\begin{bmatrix} V_1 \\ I_1 \end{bmatrix} = \begin{bmatrix} A & B \\ C & D \end{bmatrix}^m \begin{bmatrix} V_{m+1} \\ I_{m+1} \end{bmatrix}. \tag{14}$$

By applying the Floquet theorem to the voltage and the current, (13) can also be expressed as

$$\begin{bmatrix} V_{n+1}e^{\gamma d} \\ I_{n+1}e^{\gamma d} \end{bmatrix} = \begin{bmatrix} A & B \\ C & D \end{bmatrix} \begin{bmatrix} V_{n+1} \\ I_{n+1} \end{bmatrix}. \tag{15}$$

By rearranging (15), we get

$$\begin{bmatrix} A - e^{\gamma d} & B \\ C & D - e^{\gamma d} \end{bmatrix} \begin{bmatrix} V_{n+1} \\ I_{n+1} \end{bmatrix} = 0. \tag{16}$$

Because the determinant of the above matrix must be zero, we end up with the following dependence between the ABCD-parameters and the complex propagation constant γ

$$AD + e^{2\gamma d} - (A + D)e^{\gamma d} - BC = 0. \tag{17}$$

From here, we can solve the propagation constant

$$\gamma = \frac{1}{d} \ln \left(\frac{1}{2}(A + D \pm \sqrt{A^2 + D^2 - 2AD + 4BC}) \right). \tag{18}$$

If the unit cell is symmetric (i.e., $A = D$), as is often the case, this further reduces to

$$\gamma = \frac{1}{d} \ln \left(A \pm \sqrt{BC} \right). \tag{19}$$

In Section 3.2.1, the characteristic impedance of a transmission line was defined as the square root of the ratio of the immittances of an infinitesimal section Δz of the line. Because the ratio of voltages and currents in the network can vary along a unit cell in a periodic TL network, such a quantity is not suited to describe that particular system. However, the ratio at the terminals of each unit cell is constant. This constant is called the Bloch impedance, and it is defined as [29, 31]

$$Z_B = \frac{V_k}{I_k} = -\frac{B}{A - e^{\gamma d}} = -\frac{D - e^{\gamma d}}{C}. \tag{20}$$

The last two identities are obtained from (16). They can also be expressed using just the ABCD-parameters using equation (18)

$$Z_B^{\pm} = \frac{-2B}{A - D \mp \sqrt{(A+D)^2 - 4}} \tag{21}$$

or (19) for the symmetric case

$$Z_B^{\pm} = \frac{\pm B}{\sqrt{(A)^2 - 1}}. \tag{22}$$

In these expressions, the $\pm$ solutions correspond to waves traveling along the positive and negative directions of the transmission-line axis respectively. For a finite periodic cascade of two-ports terminated in a load Z_L, matching is now achieved by the conjugate matching condition $Z_B = Z_L^*$ and the reflection coefficient at the load is given by

$$\rho = \frac{Z_L - Z_B}{Z_L + Z_B}. \tag{23}$$

It can be shown that the Bloch impedance, though not the same as the characteristic impedance, does reduce to the characteristic impedance of the homogeneous TL in the homogeneity limit ($\Delta z \to 0$) [29, 31].

3.3 Dispersion diagram

A convenient way to describe the propagation of a wave inside a microwave component or a transmission line is the dispersion diagram. In a dispersion diagram the propagation constant β, i.e., the imaginary part of the complex propagation constant γ, is plotted against the free space propagation constant $k_0 = \omega/c = 2\pi f/c$. The latter variable is sometimes replaced with the frequency f or the angular frequency ω. Figure 7 shows an example of a dispersion diagram for the TE_{10}-mode of a rectangular WR-340 waveguide (inside dimensions 8.64 cm $\times$ 4.32 cm). The light line corresponds to free space propagation. It can be observed that for values $k_0 < 36.3$ 1/m (= the cut-off wavenumber for the TE_{10}-mode) there is no real solution for β, i.e., there is no propagation inside the waveguide. For $k_0 > 36.3$ 1/m, the TE_{10}-mode propagates, and for large values of k_0, β approaches the free-space propagation constant k_0.

The two velocities characterizing a wave, the phase and group velocity, can also be read from the dispersion diagram. The phase velocity is defined as [32]

$$v_p = \frac{\omega}{\beta} = c\frac{k_0}{\beta}, \tag{24}$$

and it gives the rate at which the phase of the wave propagates. In the dispersion diagram, this equals c times the slope of the line from the origin to the operating point. Therefore in Figure 7 at the cut off, the phase velocity is infinite. As k_0 increases, the phase velocity gets smaller and finally for high k_0, it equals the speed of light in vacuum.

The group velocity, in turn, is defined as [32]

$$v_g = \frac{d\omega}{d\beta} = c\frac{dk_0}{d\beta}, \tag{25}$$

and it gives the rate at which the envelope of the wave propagates. In the dispersion diagram, this corresponds simply to c times the slope of the curve at the operating point. Thus, from Figure 7 it can be read that, for all k_0, the group velocity inside the waveguide is smaller than the speed of light in vacuum, but with large k_0 the two values are approximately equal.

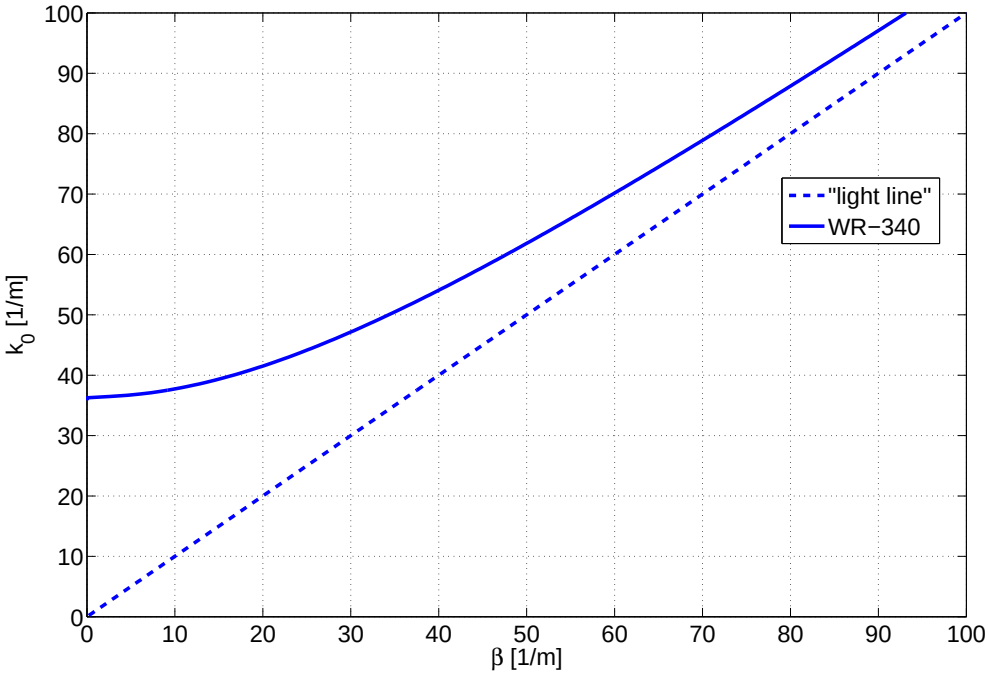

Figure 7: Dispersion diagram for the TE_{10}-mode of a rectangular WR-340 waveguide. "Light line" corresponds to free-space propagation.

3.4 Antenna theory

The IEEE defines antenna as "that part of a transmitting or receiving system which is designed to radiate or to receive electromagnetic waves" [33]. In other words, an antenna acts as a device that converts guided electromagnetic waves moving in a waveguide into free-space waves and vice versa. Antennas are usually reciprocal meaning that their properties are the same in reception and transmission. As antenna is a vital element in this thesis, in the following section the most important antenna properties are covered as well as the basics of horn antennas.

3.4.1 Far field and near field

The radiation field of an antenna or any radiating source can be divided into two regions: the near field and the far field. The near field is further divided into two regions: reactive near field and radiating near field. The approximate limit between the reactive region closest to the antenna and the radiating region, assuming that $D \gg \lambda$, is given by [34]

$$r_{nf} = 0.62\sqrt{\frac{D^3}{\lambda}}, \tag{26}$$

where D is the largest dimension of the antenna and λ is the operational wavelength. In the reactive near field, not only is part of the energy radiated to the far field, but also, due to the reactive component of the field, some of it is held back and stored near the antenna. In the radiating near field, there is no such reactive component to the field. All the energy flows towards the far field. However, the angular field distribution, i.e., the radiation pattern, depends still on the distance from the antenna. In the far field on the other hand, the angular field distribution is independent of distance as is also the ratio of the electric and magnetic fields, i.e., the wave impedance η which is approximately $120\pi\ \Omega$ in free space. Furthermore, the wave can be considered approximately a plane wave in the far field. The far-field distance is conventionally given as [34]

$$r_{ff} = \frac{2D^2}{\lambda}. \tag{27}$$

In the far field, it is also expected that conditions $r \gg D$ and $r \gg \lambda$ are satisfied. It should be noted that in reality there are no strict near-field or far-field limits. In case of the far-field condition, the field changes smoothly with distance with the perfect plane wave only attained infinitely far from the antenna. Similarly, in the near field the reactive component does not suddenly disappear at the limit given by (26) but slowly decreases as we move away from the antenna. Thus, equations (26) and (27) are only approximations which are considered to hold true in most cases with sufficient accuracy.

3.4.2 Radiation pattern

Radiation pattern gives the angular variation of radiation by a transmitting antenna. Because of the reciprocity of (most) antennas, transmitting antenna that radiates strongly to a certain direction also receives radiation from that direction efficiently. Thus, radiation patterns apply both to transmission and reception. Typically, a radiation pattern gives the radiation in the far field of the antenna.

In Figure 8, the 3-dimensional radiation pattern for one of the most common antennas, the half-wave dipole antenna, is shown. Half-wave dipole consists of a metal wire with the length of approximately half of the operational wavelength, and it is fed from a small gap in the middle of the wire. As the dipole antenna is positioned in Figure 8 along z-axis, it can be seen that this antenna radiates mostly to the horizontal plane and not at all upwards or downwards. Another way to present this radiation pattern would be to plot the E-plane and H-plane patterns as is done in Figure 9. The E-plane pattern is defined so that the E-plane contains the electric field, i.e., the electric field does not go through the E-plane. The same holds true for the H-plane and magnetic field. In the case of a dipole antenna, the E-plane is parallel to the dipole axis and the H-plane is perpendicular to it.

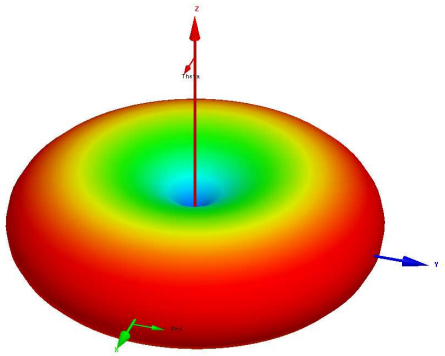

Figure 8: Radiation pattern of a half-wave dipole.

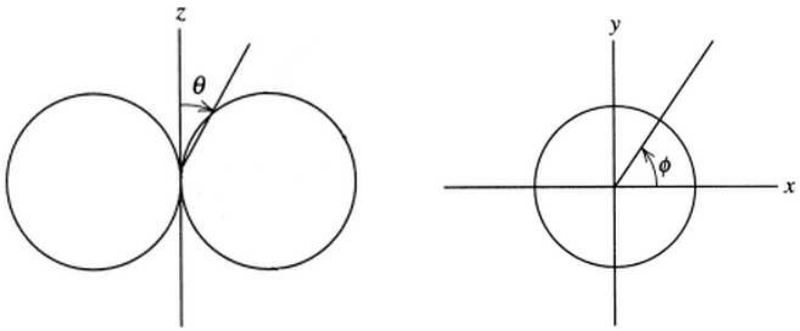

(a) (b)

Figure 9: E-plane (a) and H-plane (b) radiation patterns of a half-wave dipole [34](mod.).

3.4.3 Directivity and gain

Directivity of an antenna expresses how much greater the peak radiated power density is for an antenna than it would be if all the radiated power were distributed uniformly around the antenna. This means that a hypothetical uniformly radiating source, i.e., an isotropic source, has the constant directivity of 1. This can be expressed mathematically as [34]

$$D(\theta, \varphi) = \frac{U(\theta, \varphi)}{U_{\text{ave}}} \tag{28}$$

where $D(\theta, \varphi)$ is the directivity of the antenna in a certain direction, $U(\theta, \varphi)$ is the radiation intensity in a certain direction, and U_{ave} is the average radiation intensity. Radiation intensity is defined as the power radiated in a given direction per unit solid angle, i.e.,

$$U(\theta, \varphi) = S(r, \theta, \varphi) r^2, \tag{29}$$

where $S(r, \theta, \varphi)$ is the power density. Note that the distance dependency of the power density in the far field has the form $\propto 1/r^2$ so that the radiation intensity is independent of distance. Equation (28) gives the absolute value of the directivity though directivity is often given in decibels. Directivity, being a power ratio, is calculated in decibels as follows:

$$D_{\text{dB}} = 10 \log(D). \tag{30}$$

Somewhat confusingly, directivity can sometimes also mean, especially if no direction is specified, the maximum directivity of the antenna.

Gain or, more specifically antenna gain, is defined as 4π times the ratio of the radiation intensity in a given direction to the net power accepted by the antenna from the transmitter, i.e., [34]

$$G(\theta, \varphi) = \frac{4\pi U(\theta, \varphi)}{P_{\text{in}}}. \tag{31}$$

Unlike directivity, gain tells us not only the directive properties of the antenna but also how efficiently antenna transforms the available power to radiated power. This property can be even more easily seen in another definition for antenna gain which relates it directly to directivity:

$$G(\theta, \varphi) = e_r D(\theta, \varphi), \tag{32}$$

where e_r is the radiation efficiency, which satisfies $0 \leq e_r \leq 1$ [34]. Therefore, gain is always smaller than the corresponding directivity. Like in the case of directivity, gain is also given typically in decibels and the word "gain" can also sometimes be used as a synonym for the actual maximum gain.

For the half-wave dipole antenna introduced earlier, the (maximum) directivity and also ideally the (maximum) gain equal 1.64 or 2.15 dB. Therefore, the radiation patterns of Figures 8 and 9 can also be thought of as directivity or gain patterns by denoting the maximum of the pattern as 1.64 and the minimum as 0.

3.4.4 Polarization

The polarization of an electromagnetic wave is determined by the pattern that the instantaneous electric field traces when the wave is propagating and the direction of this tracing movement. In general, for a completely polarized wave, as opposed to unpolarized waves with random vibrations of the electric field, this pattern is an ellipse meaning that the wave is elliptically polarized. Depending on the direction of rotation, elliptical polarization can be either left-handed or right-handed. There are some important special cases to this elliptical polarization pattern which are presented in Figure 10. If the electric field moves back and forth along a line, i.e., the minor axis of the ellipse is zero, the wave is said to be linearly polarized. Two important cases of linear polarization are vertical and horizontal linear polarizations shown in Figure 10(a) and (b). If the electric field draws a circle, i.e., the minor and major axes of the ellipse are equal, the wave is said to have circular polarization as shown in Figure 10(c) and (d).

The polarization of an antenna means simply the polarization of the wave radiated by that particular antenna. However, this can change with direction. Typically, the polarization of the main beam peak is used to describe the antenna polarization. Because antennas are reciprocal, an antenna that radiates with a certain polarization also receives waves of that particular polarization most effectively, i.e., the waves couple to the antenna so that maximum possible power is received. On the other hand, if the polarizations of the antenna and the incident wave are orthogonal, ideally no power is received by the antenna. For example, vertical and horizontal linear polarizations as well as right- and left-handed circular polarizations are orthogonal to each other. A wave of any polarization can be created by combining any two orthogonally polarized waves. [35]

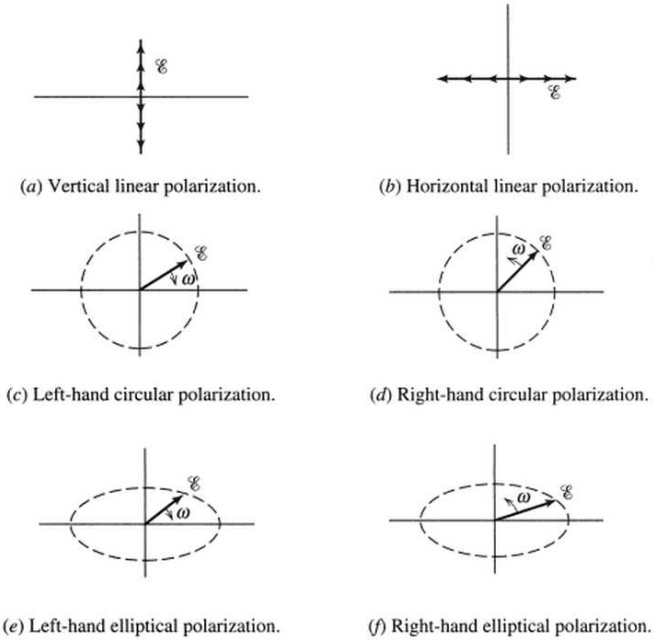

Figure 10: Polarization states [34].

3.4.5 Horn antenna

Horn antennas are very popular antennas in the microwave frequencies, especially above 1 GHz. They consist of a flaring metal waveguide giving them the shape of a horn. This flaring provides gradual transition for a wave moving in a waveguide into free space. Without the flaring, a large part of the wave would be reflected from the end of the open waveguide due to impedance mismatch between the waveguide and free space. Horn antennas are fairly directive and provide low VSWR (voltage standing wave ratio) and relatively high bandwidth due to the absence of resonant elements. Also, they are fairly lightweight and easy to construct. Furthermore, they are quite well understood meaning that accurate, though still fairly simple, analytical formulas are available [36].

The physical aperture of horn antennas, i.e., the opening through which the waves flow, is typically either circular or rectangular depending on the type of waveguide attached to the horn. Rectangular horn antennas can be further divided into H-plane sectoral horns, E-plane sectoral horns, and pyramidal horns depending on which dimension of the horn is flared or whether the horn is flared in both directions. These basic types can be seen in Figure 11.

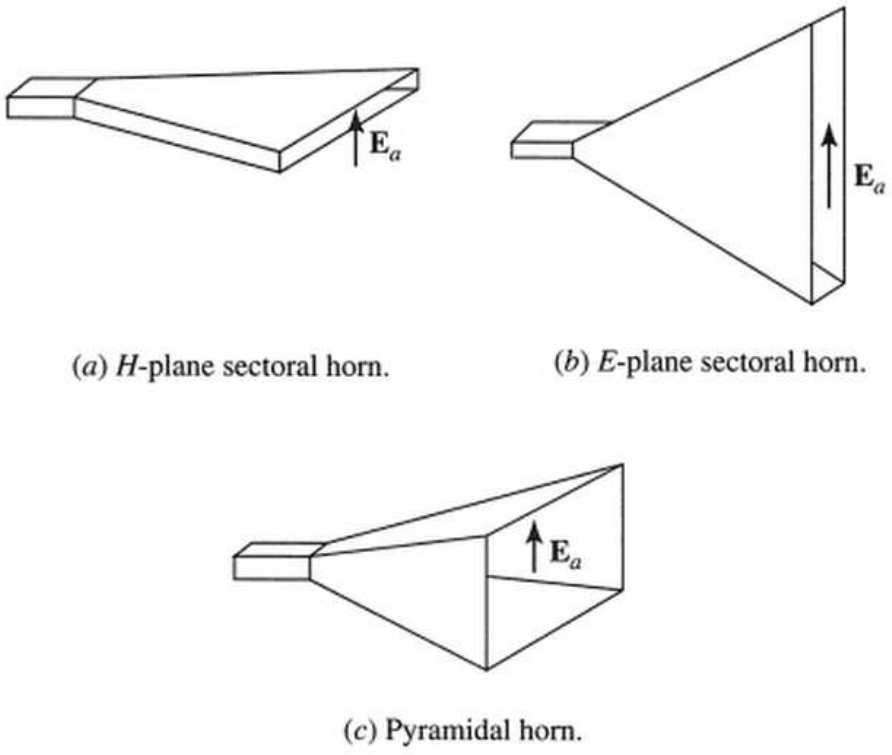

(*a*) *H*-plane sectoral horn. (*b*) *E*-plane sectoral horn.

(*c*) Pyramidal horn.

Figure 11: Different types of rectangular horn antennas [36].

Pyramidal horn is probably the most common horn antenna type. The typical geometry of a pyramidal horn is shown in Figure 12. Because pyramidal horns are flared in both the E- and H-planes, the beamwidth is narrow in both principal planes. The maximum directivity for a pyramidal horn is given by [36]

$$D_p = \frac{\pi}{32}\left(\frac{\lambda}{a}D_E\right)\left(\frac{\lambda}{b}D_H\right), \tag{33}$$

where D_E and D_H are the directivities of the corresponding E-plane and H-plane sectoral horns respectively. Analytical formulas can also be derived for these directivities [36]. Alternatively, the directivities can be read from Figure 13. It can be observed that the best directivity is obtained with a long horn having a large aperture.

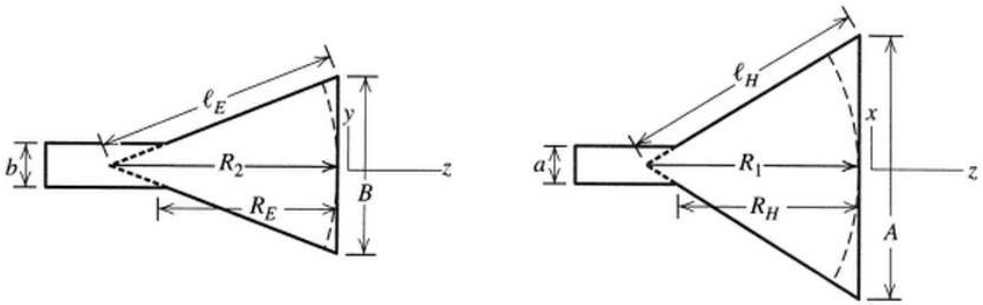

(a) (b)

Figure 12: Dimensions of a pyramidal horn: (a) E-plane view; (b) H-plane view [36].

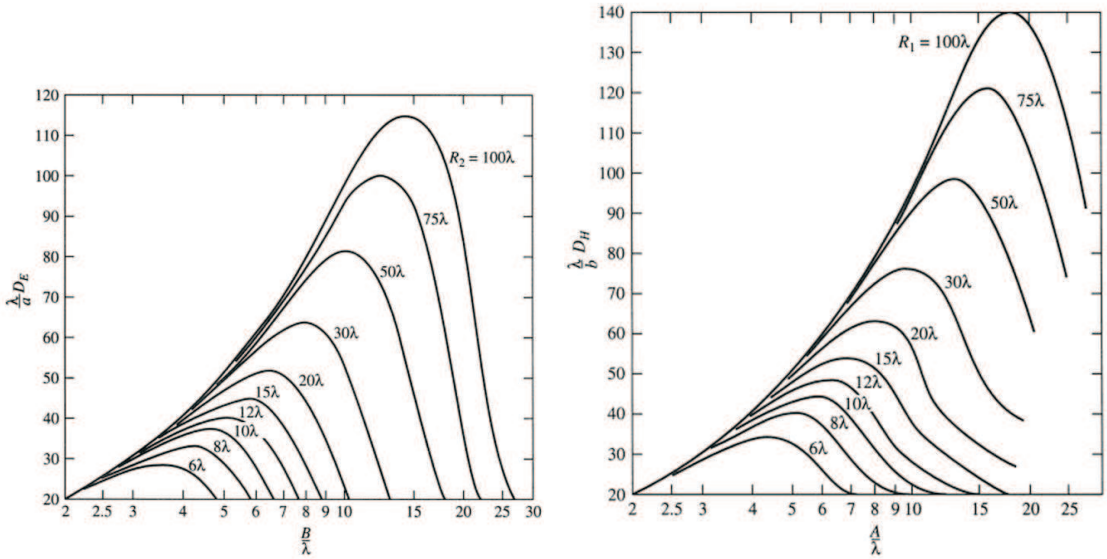

(a) (b)

Figure 13: Directivities of E-plane (a) and H-plane (b) sectoral horns [36].

Similarly, the half power beamwidths for the E- and H-plane patterns are the same as the corresponding half power beamwidths for the corresponding sectoral horns and are given by [36]

$$HP_E = 2 \arcsin \frac{0.47}{B/\lambda} \approx 54^\circ \frac{\lambda}{B} \tag{34}$$

$$HP_H = 2 \arcsin \frac{0.68}{A/\lambda} \approx 78^\circ \frac{\lambda}{A}. \tag{35}$$

From equations (34)–(35), it can be observed that the beamwidth decreases as the frequency or the size of the aperture increases. Narrower beamwidth also typically means larger directivity and gain as more of the power is directed towards the main beam direction.

Curving fins inside the horn can be used to increase the bandwidth of the antenna, similar to the ridges in a waveguide that lower the cut-off frequency. This is an especially beneficial property in reference antennas used in antenna pattern measurements allowing us to use the same antenna for measurements in a wide range of frequencies. Figure 14 shows an example of such ridged horn antenna.

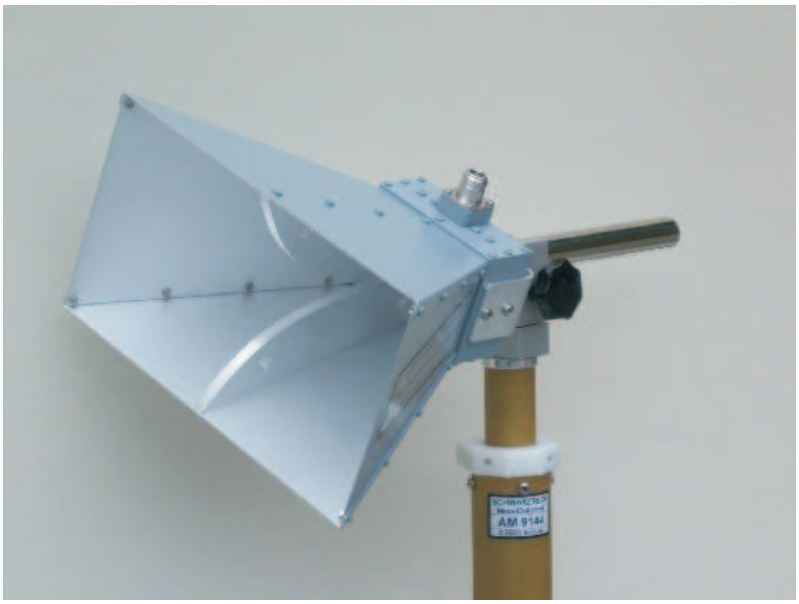

Figure 14: An example of a ridged horn antenna (Schwarzbeck BBHA 9120 D) [37].

3.5 Scattering cross section and scattering width

For a scattering object and an incident plane wave of a given frequency, polarization and direction, an area which, when multiplied by the power flux density of the incident wave, would yield sufficient power that could produce by isotropic radiation the same radiation intensity as that in a given direction from the scattering object.

Scattering cross section (or bistatic radar cross section) for an object and an incident plane wave of a given frequency, polarization and direction is defined as the area which, when multiplied by the power density of the incident wave, would yield sufficient power, which when radiated isotropically would produce the same radiation intensity as that in a given direction from the scattering object [38]. For the case when the object is equidistant from the transmitter and the receiver, this can be written as [38]

$$\sigma(\theta,\varphi) = \frac{P_r(\theta,\varphi)/\Omega}{J_i/4\pi} = \lim_{R\to\infty}\left(4\pi R^2 \frac{|E_s(\theta,\varphi)|^2}{|E_i|^2}\right), \tag{36}$$

where σ is the scattering cross section, P_r is the scattered power in a given direction, Ω is the unit solid angle, J_i is the incident power density, R is the distance between the object and the transmitter or the object and the receiver, E_s is the scattered electric field, and E_i is the incident electric field.

If we have a tall object which is either homogeneous or periodic along the longest dimension (z-axis), we can also quantify the amount of scattering by defining the scattering width of the object. Scattering width is defined using cylindrical coordinates (ρ,φ,z) as [39]

$$\sigma_{2\mathrm{D}}(\varphi) = \lim_{\rho\to\infty}\left(2\pi\rho \frac{|\mathbf{E}_s(\rho,\varphi)\cdot\hat{p}^*|^2}{|\mathbf{E}_i\cdot\hat{p}^*|^2}\right), \tag{37}$$

where $\hat{p}^*$ is the complex conjugate of the unit polarization vector $\hat{p}$. For TE waves, we have $\hat{p} = \hat{y}$ and for TM waves $\hat{p} = \hat{z}$. Ideally, (37) requires the object to be infinite in the z-direction, but the equation can also be used for the situation where the transmitting antenna is sufficiently directive and/or the object is sufficiently long that the illumination of its edges is weak compared to its center.

Scattering width is always dependent on the angle φ of the spherical coordinate system. By integrating the scattering width over φ, we get a quantity that describes the total scattering of an object, i.e.,

$$\sigma_{2\mathrm{D,tot}} = \int_0^{2\pi} \sigma_{2\mathrm{D}}(\varphi)d\varphi. \tag{38}$$

This quantity is called the total scattering width.

4 Transmission-line cloak

4.1 Principle of Transmission-line cloaking

Transmission-line (TL) cloak is an electromagnetic cloak whose operation is based on transmission-line networks. The cloak, first introduced in [5], consists of a two-dimensional or three-dimensional, loaded or unloaded, transmission-line network and a so-called transition layer surrounding it. The basic operating principle of the cloak is as follows. The wave coming from the surrounding medium couples to the transmission-line network through the transition layer. Then, the wave travels through the cloak along the transmission lines and is, on the other side of the cloak, again coupled to the surrounding medium through the transition layer. Because the wave travels through the cloak only along the transmission lines meaning that the fields are almost completely confined inside the lines, the volume between neighboring transmission lines is completely hidden from the wave, and any object planted inside this volume has no effect on the wave. This cloaking principle is demonstrated in Figure 15 for the case of a two-dimensional transmission-line network. The transmission-line network comprising the cloak is often considered a metamaterial though it does not agree with all the definitions given in Section 2.1 – another example of the vagueness of the definition.

In practical cloak designs, the transmission lines are typically symmetrical parallel-strip lines although other transmission lines can also be used. However, the practical realization of a TL network with, e.g., coaxial cables can be quite difficult. The transition layer, in turn, can be realized, e.g., by gradually enlarging the parallel-strip transmission lines and tilting them in the vertical direction so that there is no gap between adjacent cloak layers. Two examples of a practical TL-cloak design with such a transition layer can be seen in Figure 16. These are both unloaded 2D-TL-cloaks, i.e., there are neither lumped loading elements nor vertical transmission lines, which can be made volumetric by simply stacking adjacent two-dimensional layers on top of each other.

The obvious drawback of this cloaking approach is that the cloaked object has to fit inside the mesh-like transmission-line network. Therefore, the cloaked object has to be either a collection of small objects or a mesh of interconnected objects, i.e., no electrically large bulky objects can be cloaked. Furthermore, the cloaking effect is strongly mitigated when the size of the cloak approaches one wavelength at the center cloaking frequency, i.e., electrically large cloaks are not feasible. On the other hand, no exotic materials are needed making the cloak design and manufacturing fairly straightforward, at least compared to many of the alternatives presented in Chapter 2. Also, the operational bandwidth of TL-cloaks is typically fairly wide.

For perfect cloaking of an object in free space with a TL cloak, the electromagnetic wave would have to travel at the speed of light in vacuum inside the TL network. This would mean that the wave should move faster than the speed of light inside a single isolated transmission line since a single transmission line inside the network sees all the other transmission lines in the network as periodic loads which slows down the wave. This, obviously, is not possible. This problem can be

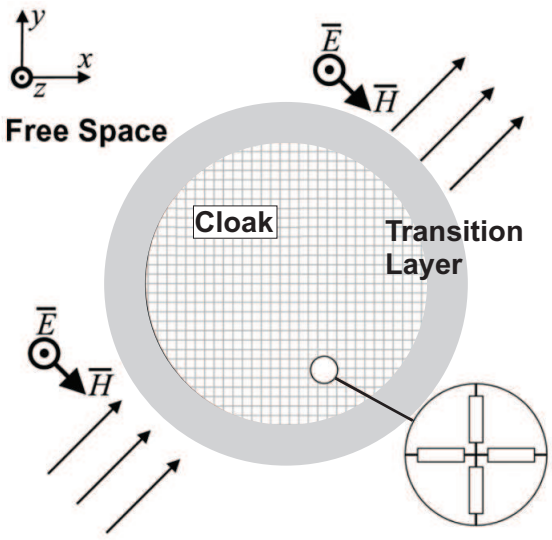

Figure 15: Basic cloaking principle.

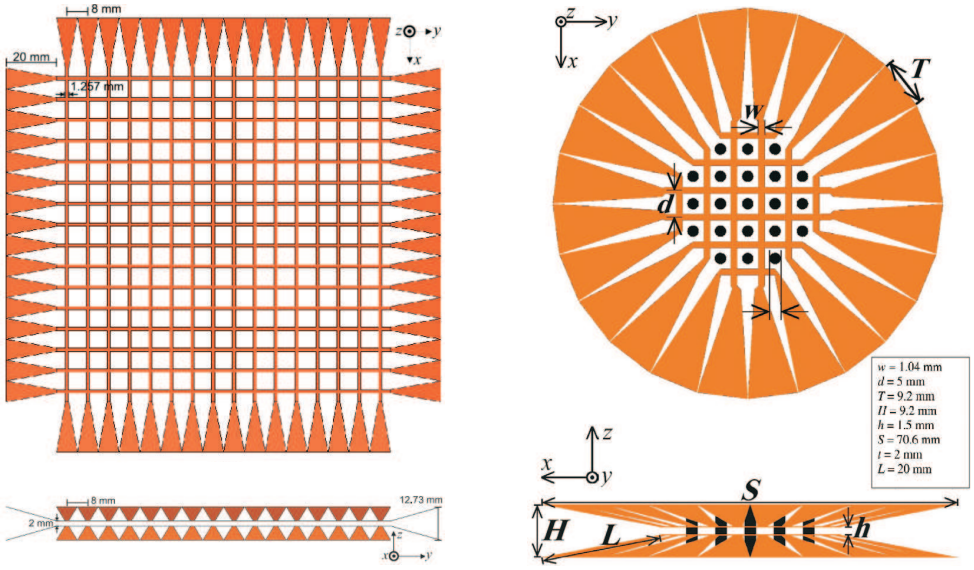

(a) (b)

Figure 16: Two examples of a transmission-line cloak:
(a) a rectangular cloak designed for 5.85 GHz frequency [6];
(b) a cylindrical cloak designed for 3 GHz frequency with a set of horizontal metal cylinders used as objects to be cloaked [40].

overcome by loading the network with periodical reactive loads [5]. However, it has been shown that for practical applications requiring large bandwidths and cloaking from signals, unloaded TL networks are preferable [5]. Although the propagation velocity is not ideal in this case, the simplicity of the design and the lack of frequency dispersion compared to the loaded TL networks make the sacrifice worthwhile.

4.2 Dispersion and impedance in transmission-line networks

The dispersion equation for the loaded 3D TL network, illustrated in Figure 17, can be fairly easily derived using basic circuit and transmission-line theory [41]. The result is for the general 3D case

$$\cos(k_x d) + \cos(k_y d) + \cos(k_z d) = \frac{Y}{2S} - 3\frac{K}{S} \tag{39}$$

and for the 2D case

$$\cos(k_x d) + \cos(k_y d) = \frac{Y}{2S} - 2\frac{K}{S}, \tag{40}$$

where

$$S = \frac{Z}{(ZA_{\mathrm{TL}} + B_{\mathrm{TL}})(ZD_{\mathrm{TL}} + B_{\mathrm{TL}}) - B_{\mathrm{TL}}^2}, \tag{41}$$

$$K = \frac{Z(A_{\mathrm{TL}}D_{\mathrm{TL}} - B_{\mathrm{TL}}C_{\mathrm{TL}})(ZA_{\mathrm{TL}} + B_{\mathrm{TL}})}{((ZA_{\mathrm{TL}} + B_{\mathrm{TL}})(ZD_{\mathrm{TL}} + B_{\mathrm{TL}}) - B_{\mathrm{TL}}^2)B_{\mathrm{TL}}}, \tag{42}$$

and A_{TL}, B_{TL}, C_{TL} and D_{TL} form the ABCD-matrix of a transmission-line section

$$\begin{bmatrix} A_{\mathrm{TL}} & B_{\mathrm{TL}} \\ C_{\mathrm{TL}} & D_{\mathrm{TL}} \end{bmatrix} = \begin{bmatrix} \cos(k_{\mathrm{TL}}d/2) & jZ_{\mathrm{TL}}\sin(k_{\mathrm{TL}}d/2) \\ jZ_{\mathrm{TL}}^{-1}\sin(k_{\mathrm{TL}}d/2) & \cos(k_{\mathrm{TL}}d/2) \end{bmatrix}. \tag{43}$$

In (39)–(43), k_x, k_y, and k_z are the propagation constants along the corresponding axes inside the TL network with the total propagation constant being $k = \sqrt{k_x^2 + k_y^2 + k_z^2}$, d is the period of the network, Y is the lumped shunt admittance, Z is the lumped series impedance, Z_{TL} is the characteristic impedance of the transmission line, and k_{TL} is the propagation constant of the transmission line. In the case of an unloaded 2D transmission-line network (with $Y \to 0$ and $Z \to 0$), (40) further reduces to

$$\cos(k_x d) + \cos(k_y d) = 2\cos(k_{\mathrm{TL}}d). \tag{44}$$

If we have $k_y = 0$ and $k_x = k$ meaning that the propagation is only along one axis, we get

$$\cos(kd) = 2\cos(k_{\mathrm{TL}}d) - 1. \tag{45}$$

Obviously, similar formula is also true for k_y if we choose $k_x = 0$ and $k_y = k$. Furthermore, if we assume that $k_{\mathrm{TL}}d$ is small and use the approximation based on the Taylor series

$$\cos(x) = 1 - \frac{x^2}{2!} + \frac{x^4}{4!} - \frac{x^6}{6!} + \ldots \approx 1 - \frac{x^2}{2!}, \tag{46}$$

we get that

$$\cos(kd) \approx 1 - k_{\mathrm{TL}}^2 d^2. \tag{47}$$

If we apply (46) again to the left side of (47), we get simply that

$$k \approx \sqrt{2} k_{\mathrm{TL}}. \tag{48}$$

It is worth noting that if we have $k_x = k_y = \frac{1}{\sqrt{2}} k$, i.e., the propagation is diagonal relative to the transmission lines, we also get, though now without any approximations, $k_x = k_y = k_{\mathrm{TL}}$ or alternatively $k = \sqrt{2} k_{\mathrm{TL}}$. In other words, if the period of the TL network is small enough compared to the wavelength, the wave propagates in the TL medium the same way no matter what the propagation direction is.

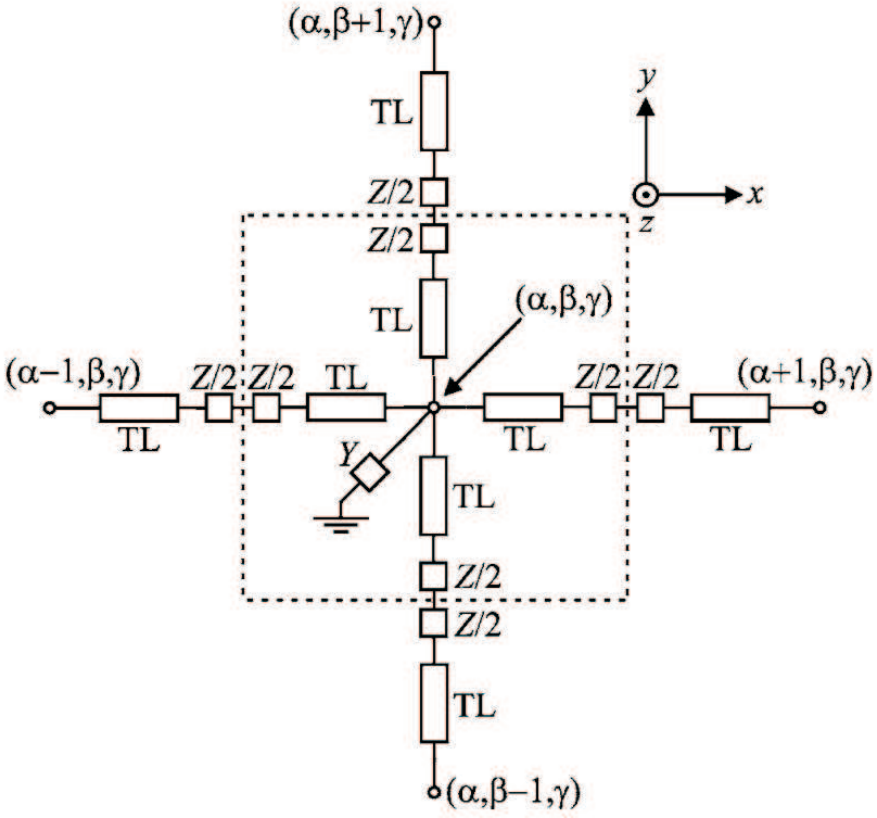

Figure 17: Unit cell of a loaded TL network [41]. The transmission lines and impedances along the z-axis are not shown.

4.3 Previous measurement results

In contrast to many cloaking techniques introduced in Chapter 2, there has not only been a wealth of numerical results on the topic of TL-based cloaking but also quite a lot of experimental studies. First experimental results for the TL-cloak were shown in [6]. Though the TL-cloak had been introduced earlier in [5], no measurement results were shown in that publication. In [6], the rectangular cloak of Figure 16(a) was manufactured. The cloak was designed for the frequency 5.5 GHz, i.e., at 5.5 GHz the impedance matching with free space was optimal. The cloak was placed inside a parallel-plate waveguide with plates lying along the xy-plane. According to the image principle, this corresponds to the case where the cloak consisting of TL-cloak layers shown in Figure 16(a) is effectively infinitely periodic in the z-direction. The object to be cloaked was an array of effectively infinitely long metal rods that fit inside the TL-network. The measurement setup can be seen in Figure 18. A coaxial feed probe placed inside the waveguide was used for exciting a cylindrical wave inside the waveguide. A measurement probe was placed above the top part of the waveguide. The transmission between these two probes was then measured in various positions along the grid using a vector network analyzer (VNA). The measurement results for the empty waveguide, uncloaked object inside the waveguide, and the cloaked object inside the waveguide at 5.85 GHz can be seen in Figure 19. Clearly, at this frequency the cloak works as intended, guiding the wave around the metal rods leading to an electric field distribution very similar to the one measured with the empty waveguide. The array of metal rods, on the other hand, clearly distorts this distribution on both sides of the object.

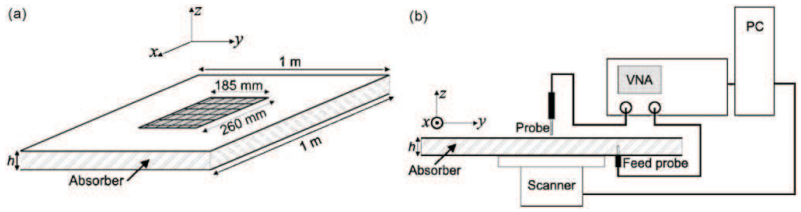

Figure 18: Measurement setup: (a) waveguide with a metal grid on the upper plate, (b) measurement system with a VNA connected to the feed and measurement probes and a PC controlling the scanner which moves the waveguide in x- and y-directions [6].

Frequency response of an actual cylindrical volumetric cloak has also been investigated in a rectangular waveguide environment [8, 40]. Four layers of the cloak shown in Figure 16(b) which was designed for the operational frequency of 3 GHz were manufactured and stacked on top of each other. The cloaked object was an array of vertical metal rods, causing a short-circuit in the waveguide, connected periodically to each other with a set of metal cylinders. The transmission lines were separated from each other and from the cloaked object using dielectric foam with relative permittivity $\epsilon_r \approx 1.05$. The transmission through the rectangular waveguide was measured in three cases: with the cloaked object placed inside the waveguide,

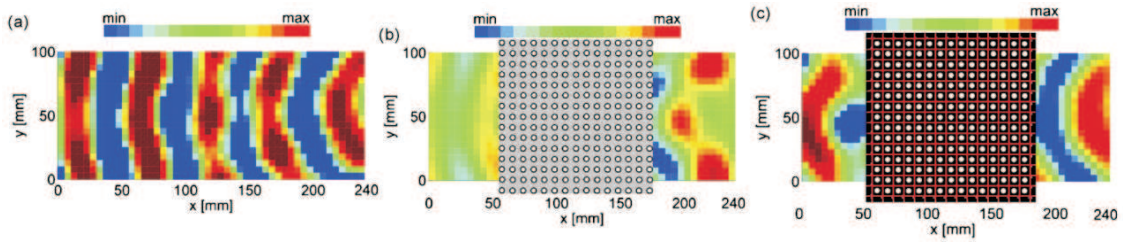

Figure 19: Measured time-harmonic electric field distribution at 5.85 GHz; (a) empty waveguide, (b) reference object inside the waveguide, (c) reference object and the transmission-line network inside the waveguide. The transition layer is not shown in (c) for clarity [6].

with the uncloaked object placed inside the waveguide, and with the empty waveguide. The results can be seen in Figure 20. With the bare reference object placed inside the cloak, hardly any power is transmitted through the waveguide whereas with the cloaked object, the magnitude of the transmission coefficient is very close to the corresponding value when the waveguide is empty. The slight difference in the phase is due to the non-ideal wavenumber inside the cloak. In conclusion, the cloak works as expected even in a realistic scenario with all the errors from manufacturing and manual assembly present.

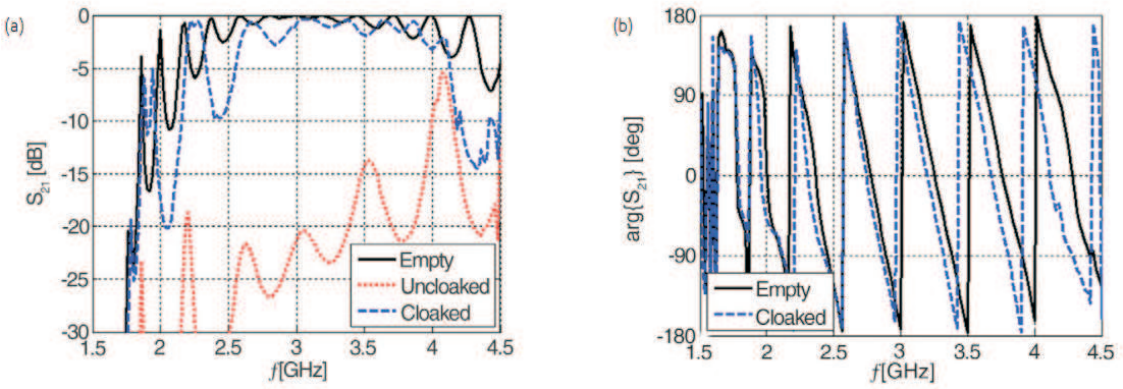

Figure 20: Measured transmission results for the cloak of Figure 16(b) placed in a waveguide: (a) Measured transmission magnitude for the empty waveguide, waveguide with the uncloaked object inside and the waveguide with the cloaked object inside; (b) Measured transmission phase for the empty waveguide and the waveguide with the cloaked object inside [40].

5 Designing and manufacturing a novel transmission-line cloak

5.1 Designing a novel TL-cloak

The first goal of this thesis is to make a new cloak design based on the earlier cylindrical two-dimensional TL-cloak designs [7, 8, 40, 42], but with increased emphasis on simplicity and ease of manufacture and assembly. Two major changes are made to the basic design of Figure 16(b). Firstly, the transition layer which consisted of a set of gradually widening strips in the earlier studies is replaced with a set of solid conical metal layers. Secondly, the transmission-line networks are printed on a substrate layer using well-established printed circuit board (PCB) technology as opposed to using separate grids of metal strips. The substrate material used is Rogers RT/Duroid 5880 [43] with $\epsilon_r = 2.2$ and the loss tangent of 0.0009, and the insulating and supporting layer between the transmission line strips is chosen to be Rohacell 71 WF [44] with $\epsilon_r = 1.07$ and the loss tangent of 0.0003. Finally, the operational frequency of the cloak is chosen to be 3 GHz. This choice was made based on the properties of the available antennas and the anechoic chamber where the final measurements were to be conducted.

In [7, 45], the object to be cloaked was a set of infinitely long vertical metal rods placed inside the transmission-line grid. However, in practical applications it would be beneficial if the object to be cloaked could be a fully three-dimensional mesh-like object. This idea is implemented by joining the vertical metal rods together with a periodical set of thin metal cylinders, similar to [40]. It was shown in [42] that such a metal cylinder inside the cloak does not affect the operation of the cloak because practically no fields reach the volume occupied by these cylinders.

The cloak dimensions are optimized using a commercial full-wave electromagnetic simulation software Ansys HFSS (High Frequency Structure Simulator) which utilizes the finite element method [46]. This is done by modeling a fourth of a single layer of the TL-cloak and applying appropriate symmetry boundary conditions as illustrated in Figure 21. Using symmetry boundaries is an easy way of simplifying any computational model where there is some kind of symmetry. Symmetry boundaries represent perfect E or perfect H planes of symmetry, i.e., symmetry planes where the electric field is, respectively, perpendicular or parallel to the surface. Behind every symmetry boundary one can imagine there being a mirror image of the model. Thus, by applying the E-field symmetry boundary conditions to the top and bottom surfaces the cloak is made effectively infinitely periodic in the z-direction as the E-field is parallel to z-axis. Applying the H-field symmetry boundary condition to the vertical surface next to the symmetrical scatterer, on the other hand, allows us to simulate only one half of the real computational space, thus reducing the simulation time significantly. The remaining outer boundaries are assigned as radiation boundaries which allow waves to radiate to the far field without reflections from the surface. In the simulation, the cloak with the object inside is illuminated with a plane wave with the electric field pointing to the $+z$-direction and the wave vector to the $+x$-direction. Corresponding simulation is also conducted for the bare

uncloaked object. In order to quantify the cloaking effect, the normalized total scattering width is calculated in the xy-plane, i.e., for $\theta = 90°$, for the frequency range of 1 GHz – 5 GHz. This is done by, first, using the intrinsic HFSS-function to calculate the bistatic radar cross section as a function of φ-angle for each frequency and then simply summing up the φ-components using MATLAB. Finally, the ratio of the two total scattering cross sections is plotted as a function of frequency. This quantity can also be thought of as the ratio of the scattering widths, as can be seen by comparing equations (36) and (37), which may be a more appropriate definition as we are now effectively considering infinitely long objects.

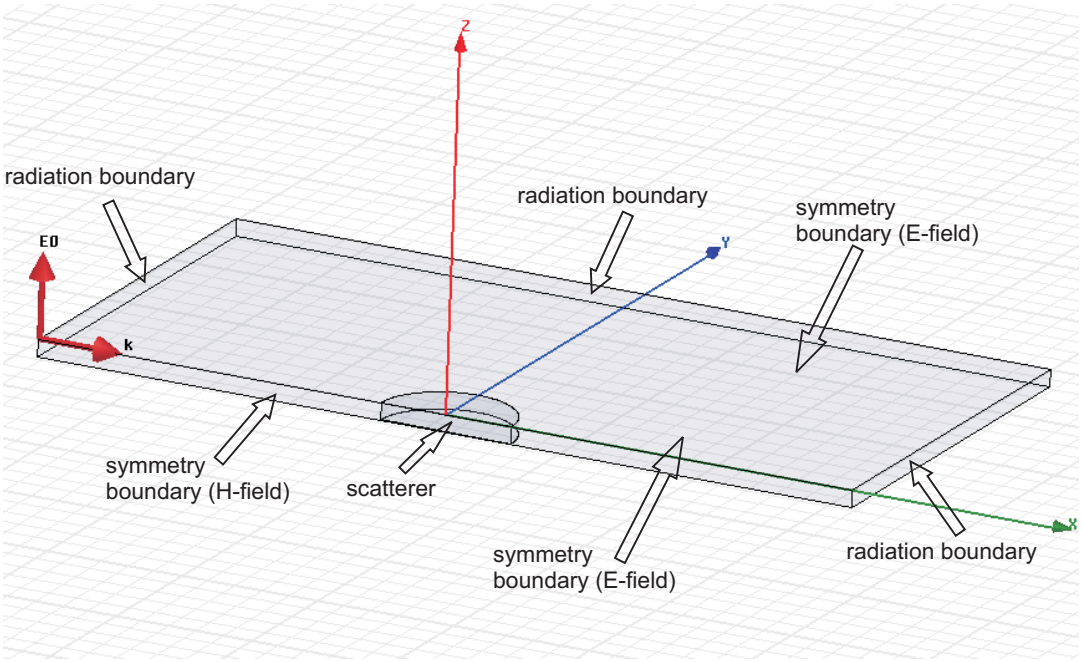

Figure 21: Basic simulation model.

The structure is optimized in a variety of ways. Firstly, the cloak presented in [7] is simulated with the transition layer consisting of a set of gradually widening strips replaced with a set of solid conical metal layers. Also, in this simulation the metal reference object with some tentative dimensions is added to the model as are also the Rogers RT/Duroid 5880 and Rohacell substrates. The geometry of the cloak is presented in Figure 22. Secondly, based on the results of the first simulation, the whole model is scaled in proportion to the wavelength in order to shift the operational frequency to the wanted 3 GHz frequency. Thirdly, the length of the coupling layer is optimized. Fourthly, the dielectric materials used (Rohacell and Rogers RT/Duroid 5880) are only supplied in certain standard thicknesses which has to be taken into account in the final vertical dimensions of the cloak. The thicknesses of the metal cylinders of the object to be cloaked are adjusted to accommodate this change in the vertical dimensions without changing the height of the whole structure. Finally, the radius of the cloaked object's metal cylinders is optimized in order to further improve the normalized scattering width.

It is noteworthy that during the simulation process the new coupling layer design

was observed to have markedly different behavior compared to the one based on widening metal strips. As the thickness of the transition layer increases, the cloaking effect is improved with practically no shift in the operational frequency, as shown in Figure 23, unlike in the case of strip transition layer where increasing the thickness of the transition layer causes the operational frequency to shift down considerably [45]. That is also the reason why the length of the coupling layer in the final design, 68 mm, is much greater than in the earlier cloak designs utilizing gradually enlarging strips for coupling [5–8, 42]. The cloaking effect could be even further improved by further increasing the radius of the transition layer though a very long transition layer would make the cloak impractical.

The final dimensions of the cloak can be seen in Table 1, and the final simulated normalized total scattering width as a function of frequency is drawn with a solid line in Figure 23. At the operational frequency of 3 GHz, the normalized total scattering width is as low as 0.068, that is, due to the cloak the normalized total scattering by the object is decreased by over 93 %. Furthermore, the cloaking effect is very wideband with a 6 dB bandwidth, corresponding to normalized scattering width of 0.25, of about 1.7 GHz. As the measurements conducted with the cloak would be free space measurements, the final cloak needs to be fairly tall electrically. Thus, the cloak to be manufactured is chosen to consist of 20 TL-layers on top of each other making the total height of the cloak 240 mm. This cloak design with the dimensions of Table 1 was reported in [47].

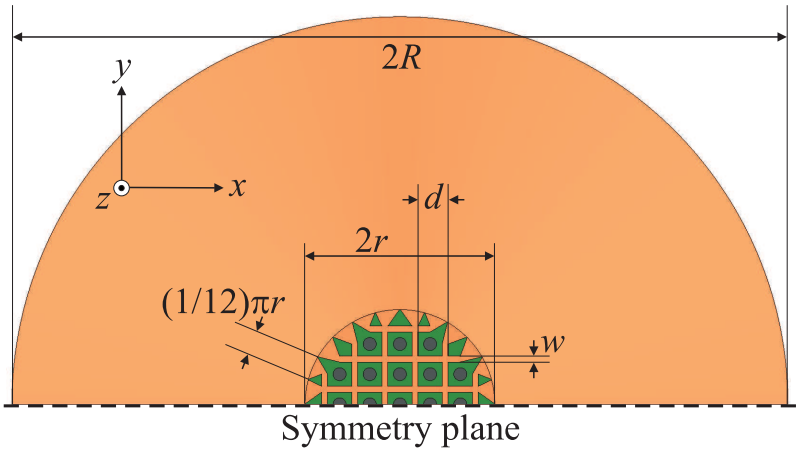

(a)

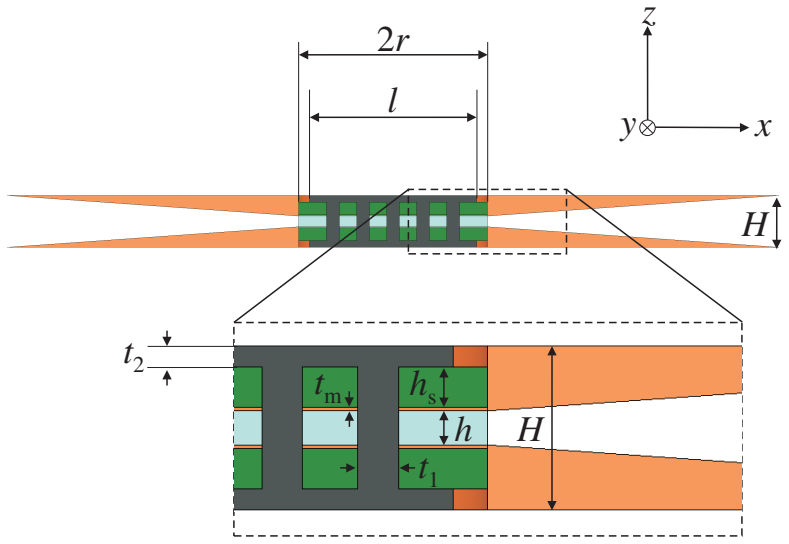

(b)

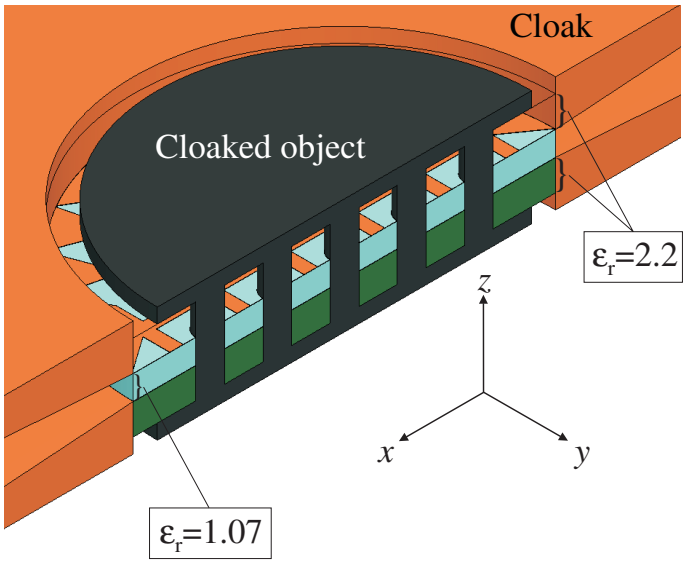

(c)

Figure 22: Cloak geometry for one half of a single cloak layer: (a) xy-plane view; (b) xz-plane view; (c) cut along xz-symmetry plane (the upper substrate is invisible).

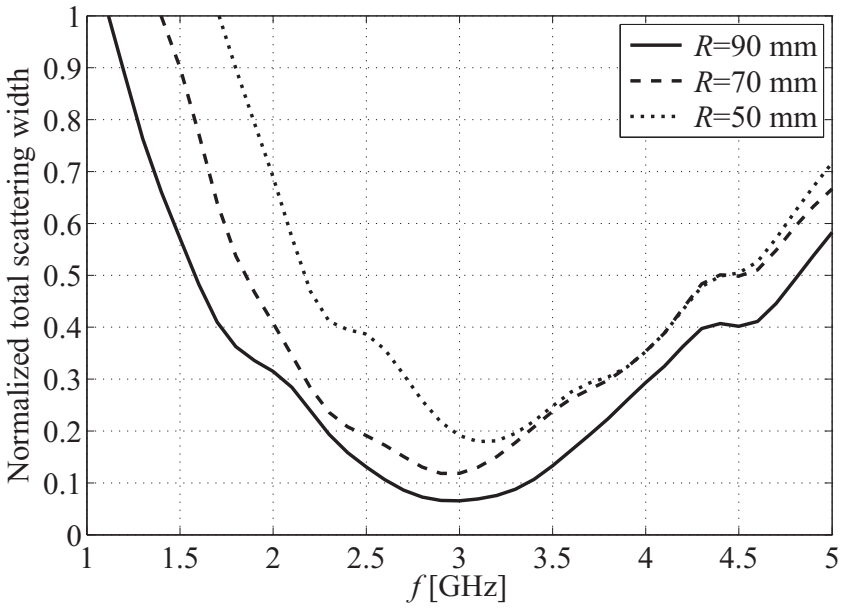

Figure 23: Simulated normalized total scattering widths for three different transition layer lengths (the other dimensions according to Table 1).

Table 1: Dimensions of the cloak.

d	7 mm	H	12 mm	t_m	0.035 mm
w	1.4 mm	r	22 mm	t_1	3 mm
h	2.5 mm	R	90 mm	t_2	1.54 mm
h_s	3.175 mm	l	39 mm		

As the transmission-line network is unloaded and air-filled, we have $Y = 0$, $Z = 0$ and $k_{\mathrm{TL}} = k_0 = 2\pi f/c$. Therefore, the dispersion curve for the two-dimensional transmission-line network with the dimensions of Table 1 can now be calculated using (44). The resulting dispersion curve for the case when the transmission lines are parallel/perpendicular to the direction of propagation is presented in Figure 24 and the corresponding phase and group velocities calculated using (24) and (25) in Figure 25. As was predicted in Section 4.2, the dispersion curve is linear in the lower frequencies with $k = \sqrt{2}k_0$. This line also corresponds to the general solution for the case when the transmission lines are diagonal to the direction of propagation, as shown in Section 4.2. Furthermore, it can be observed that for low frequencies the group and phase velocities are equal and have the value $c/\sqrt{2} \approx 0.7071\ c$, but as the frequency increases the phase velocity decreases in a much slower pace than the group velocity. Finally, at approximately 10.7 GHz which corresponds to the quarter-wave resonance of the period d, the group velocity tends to zero and the phase velocity has the value 1.499×10^8 m/s $\approx 0.5\ c$. At the operational frequency of 3 GHz, the phase velocity is 2.102×10^8 m/s $\approx 0.701\ c$ and the group velocity is 2.066×10^8 m/s $\approx 0.689\ c$.

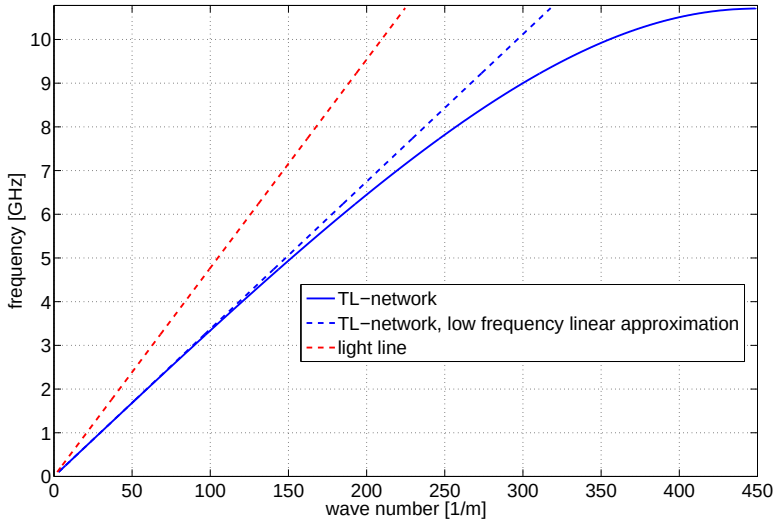

Figure 24: Dispersion diagram for the designed transmission-line network (dimensions of Table 1) when the transmission lines are parallel/perpendicular to the direction of propagation. "Light line" corresponds to free-space propagation.

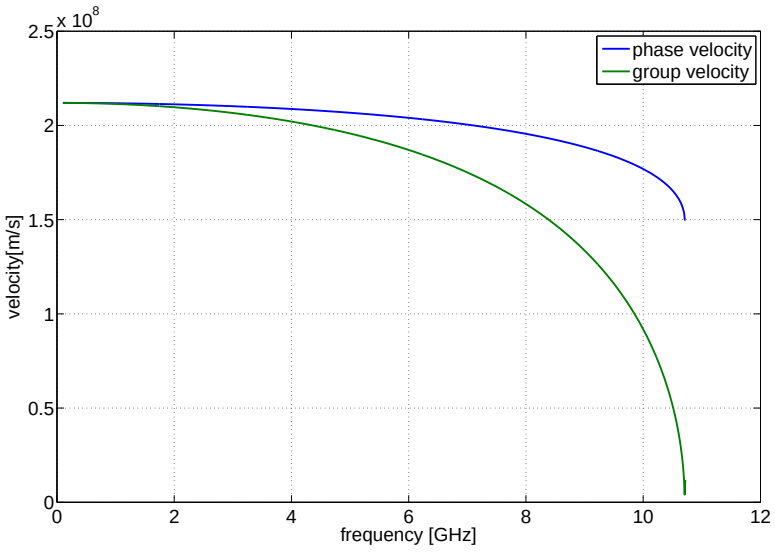

Figure 25: Phase and group velocities for the designed transmission-line network (dimensions of Table 1).

5.2 Manufacturing the cloak and the object to be cloaked

As described before, the dimensions of the cloak are determined using computer simulations. The final dimensions for the cloak can be seen Table 1 and the final geometry in Figure 22. Already during the simulation process, the material for the transmission-line PCB and the layer separating the TL strips from each other were chosen to be Rogers RT/Duroid 5880 and Rohacell 71 WF, respectively. Nevertheless, the metal used for the cones forming the transition layer of the cloak was still to be chosen. The first option was to use brass for the metal cones which was known to be suitable for soldering. This was important because the PCB had to be soldered to the metal cone and this connection had to be strong enough to be able to support the weight of the metal cone. Therefore, a prototype of a brass cone was manufactured. However, the result was not very satisfactory. During the machining process the metal was bent due to the softness of brass causing the final product to be slightly bent. Also, the weight of the brass cone was measured to be 435.6 g. As the final cloak would consist of 40 of these cones in addition to other parts, the full brass cones were deemed to be impractical for our purposes. A lighter metal was needed. Aluminum was thought to be a good candidate with density of 2700 kg/m^3 compared to the density of brass being $8300 - 8700$ kg/m^3. The problem is that conventional tin-based solder does not operate with aluminum. Though soldering aluminum is possible, the thin invisible coating of aluminum oxide covering any aluminum surface and the high temperature needed make it a fairly complicated process. This problem was solved by inserting a 2 mm thick brass ring inside the aluminum cone so that the combined dimensions were equal to those determined using simulations. The brass ring was attached simply by taking advantage of the thermal expansion property of metals. By heating the aluminum and cooling the brass ring, the brass ring which was manufactured to be slightly larger than the hole inside the aluminum cone at room temperature could be easily inserted inside the aluminum cone. When the temperatures of the metals would even out back to room temperature, the brass ring would be jammed inside the aluminum cone. A prototype of this new cone type was manufactured. It was measured to weigh only 150.0 g, a considerable improvement over the full brass cone. The final machining of the metal cones as well as the metal cylinders, still made of brass, needed for the object to be cloaked was done by Precia [48], the etching and cutting of the PCBs by Prinel Piirilevy Oy [49] and the manufacturing of the metal (steel) rods also needed for the object to be cloaked by Pertik Oy [50]. The final parts are shown in Figures 26 and 27. The needed Rohacell discs with an array of holes were manufactured in-house. Rohacell discs with height equal to the combined height of one of the aforementioned Rohacell discs and two PCB layers were also manufactured and used for the bare reference object to separate the metal cylinders from each other.

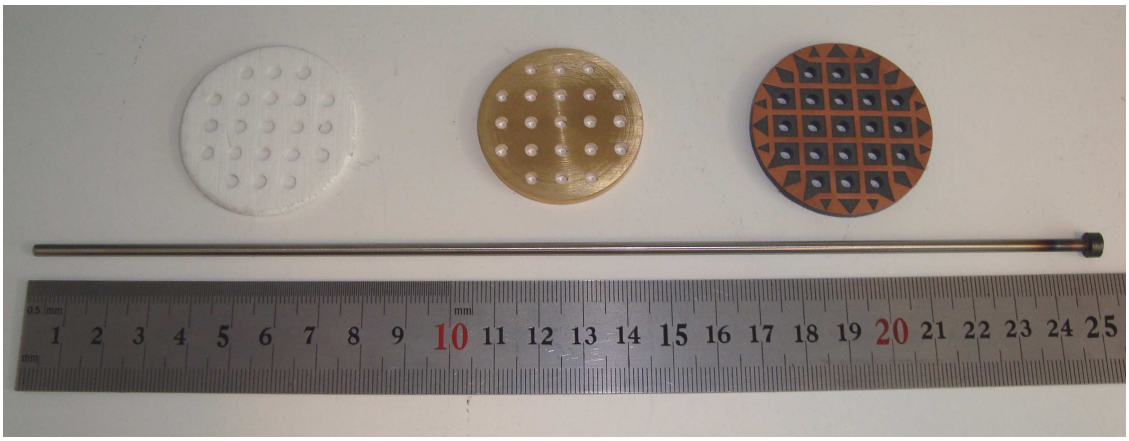

Figure 26: Cloak parts (from left to right): Rohacell insulator, metal cylinder, PCB, and metal rod. Two metal cylinders with half the thickness of the one pictured were also manufactured for the both ends of the structure.

Figure 27: Aluminum cone with a brass ring.

Once all the parts had been manufactured, the cloak and the reference object still had to be assembled. First, the PCBs were soldered to the metal cones. Because essentially the whole aluminum cone had to be heated in order to heat the brass ring, a heating plate had to be utilized for generating enough heat. Also, special solder, which contained not only tin and lead but also silver, was used in order to make the bond as strong as possible. The soldering station setup is shown in Figure 28 and a soldered PCB in Figure 29. The cloak was assembled simply by sliding the PCBs, the metal cylinders and the Rohacell discs through the metal rods one by one forming the geometry of Figure 22. However, when assembling the cloak, it was soon noticed that because the holes in the PCBs and metal cylinders had been made exactly the same size as the metal rods, extensive force had to be used in sliding the cloak layers through the metal rods which caused many of the solderings to break. In order to make the assembly easier, the holes on the metal cylinders and the PCBs were enlarged slightly. The bare reference object was assembled in a similar fashion with the PCBs replaced with Rohacell. The final assembled cloak with cloaked object inside can be seen in Figure 30 and the corresponding object without the cloak in Figure 31. As can be seen from Figures 30 and 31, the metal cylinders are not aligned in a perfectly same way in the two objects. The cloak is about half a centimeter taller than the bare reference object, excluding the vertical metal rods which are the same height in both cases. This extra height is probably due to the bulkiness of the soldering which increased the height of each TL-layer slightly. The effect of this imperfection on the measurements should be expected to be minor.

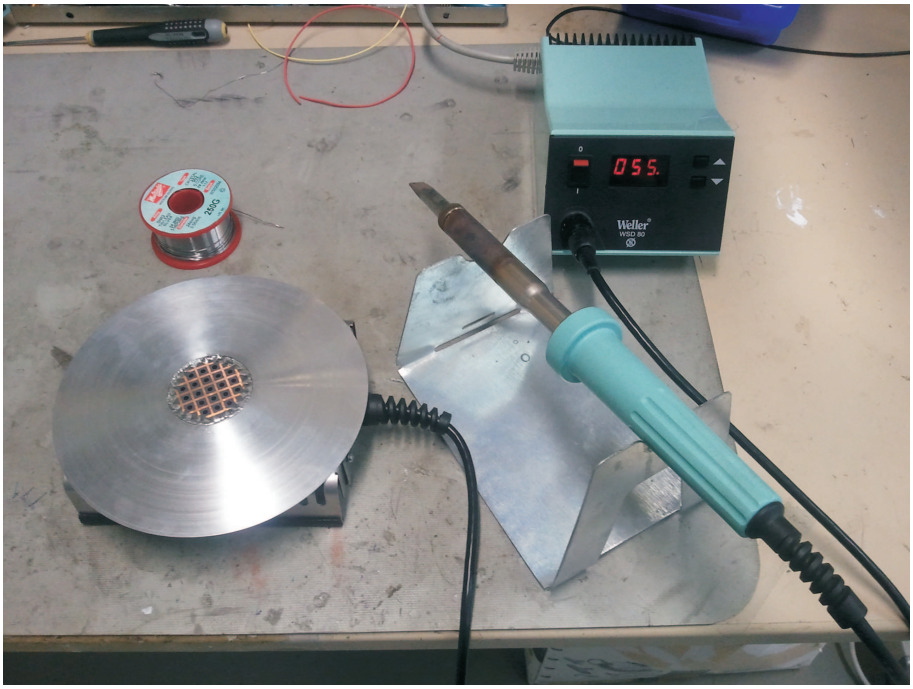

Figure 28: Soldering setup.

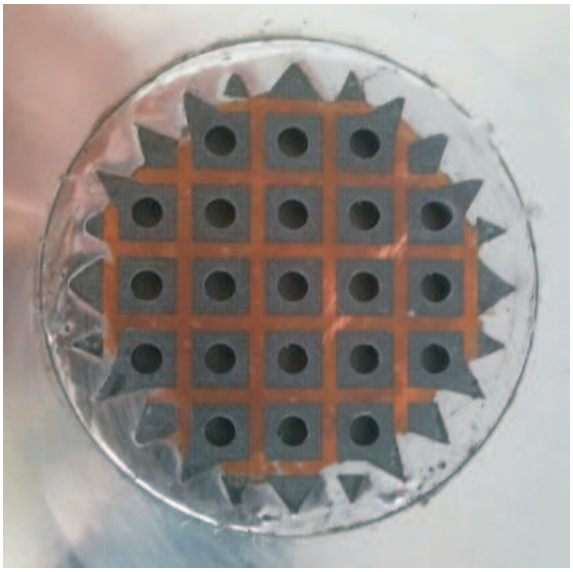

Figure 29: PCB soldered to an aluminum cone with a brass ring in the center.

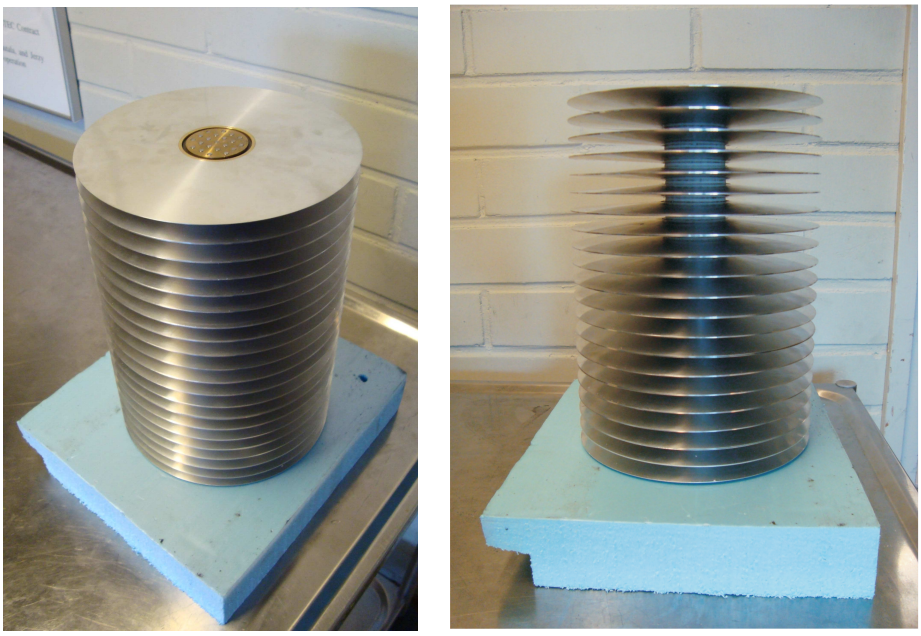

(a) (b)

Figure 30: Finished cloak with the cloaked object inside.

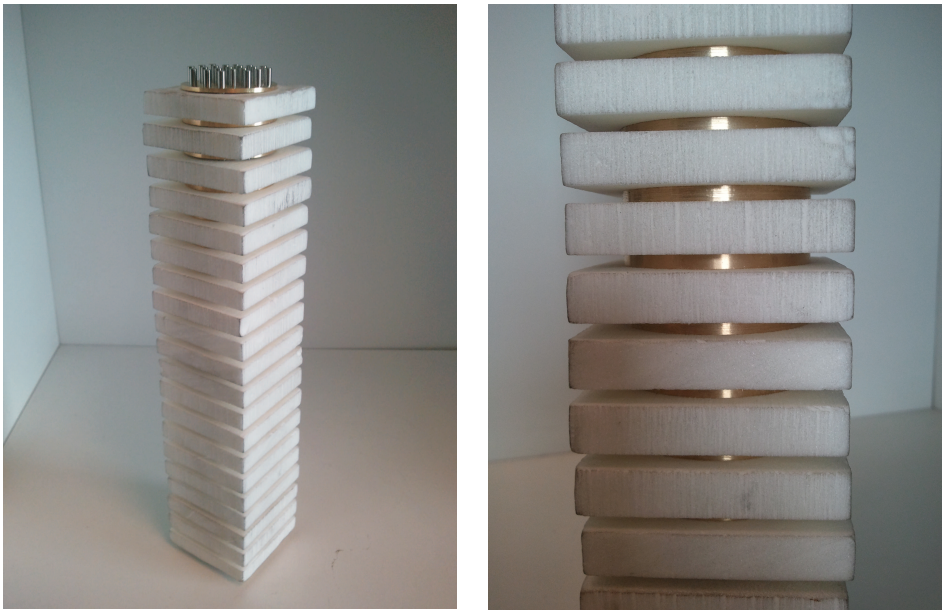

(a) (b)

Figure 31: Bare reference object.

6 Measurements

In Section 4.3, some previous measurement results for transmission-line cloaks were covered. All of these previous measurements were conducted inside a waveguide of some sort. Though these types of measurements demonstrate quite effectively the properties of the cloak, the setup is, in a way, quite artificial meaning that it is quite far from the practical applications of the device. Most likely a cloak would not be used inside a waveguide but in free space. Although in some cases the waveguide was used to simulate a free space scenario, in these cases the cloak was also effectively infinite which, again, does not represent the real applications very well. In this thesis, the goal is, for the first time, to do TL-cloak measurements in a true free space environment by studying the antenna blockage caused by the cloaked object and the bare reference object placed in the near field of an antenna. In this chapter, the measurement setup and the measurement procedure are covered as well as the basics of radiation pattern measurements in an anechoic chamber.

6.1 Radiation pattern measurements

Maybe the most straightforward, or at least the most intuitive, way of measuring the radiation pattern of any antenna would be to transmit with the antenna under test (AUT) and measure the received power level around the antenna over a sphere of constant radius using another antenna. However, this would be quite impractical and cumbersome, often requiring us to manually move the measurement antenna, hereafter called the instrumentation antenna. That is why, typically in a radiation pattern measurement, the concept of antenna reciprocity is utilized. Because any antenna works similarly both in transmission and reception, we can, instead of moving the receiving instrumentation antenna around the transmitting AUT, keep the instrumentation antenna static and use it for transmission while rotating the AUT, now used for reception, around its axis. This way we can be sure that the distance between the two antennas stays constant. Also, now the movement, i.e., the rotation of the AUT, can be easily done using an electronically controlled rotating stand. In order to fully disclose the radiation pattern of any given antenna, the antenna would have to be rotated so that all the possible angles (θ,φ) are covered which, though possible, is quite time-consuming and therefore rarely done. Usually, the principal plane patterns, i.e., the E- and H-plane patterns, give us sufficient information about the full radiation pattern.

6.2 Anechoic chamber

Radiation pattern measurements are often conducted in an anechoic chamber. Anechoic chamber is a room completely lined with RF (radio frequency) absorbing material. The idea is to suppress reflections from the floor, the ceiling and the walls so that the room acts effectively as a free-space environment. Typically to achieve this, the room is also shielded against external disturbances by an additional metal layer under the absorbing material. At microwave frequencies, the absorbing ma-

terial is typically made of polyurethane foam impregnated with carbon particles in order to increase the losses. The foam is usually in the shape of pyramids or wedges as shown in Figure 32. The thickness of this foam coverage determines the lowest operational frequency of the room as the thickness of the absorbers should be several wavelengths. At frequencies below 1 GHz, the polyurethane absorbers would have to be quite thick which is why electrically thinner lossy ferrite tiles are preferred at these frequencies. The main advantage of using an anechoic chamber instead of other antenna range options, for example an outdoor range, is that the measurement can be done indoors in a controlled environment. Also compared to near-field range measurements, the anechoic chamber measurements are simpler, less time-consuming and less susceptible to measurement errors due to misalignment though more space and absorbers are needed. [51, 52]

As reflections from the environment are often the most significant source of error in an antenna measurement, the quality of an anechoic chamber is determined by its reflectivity level. The reflectivity level R is the ratio of the field strengths of the reflected wave E_r and the directly transmitted wave E_d in decibels:

$$R = 20 \log \left(\frac{E_r}{E_d} \right). \tag{49}$$

Reflections cause errors especially in measurement of antenna pattern's sidelobes. Also, the error grows as the directivity of the transmitting antenna decreases. [51]

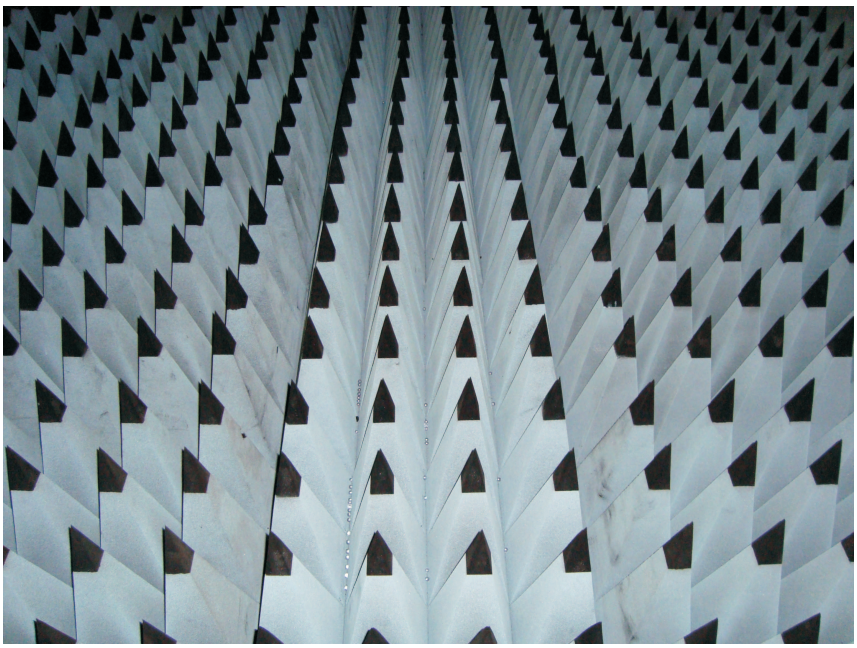

Figure 32: Urethane foam pyramids used in the microwave frequencies to absorb the incident waves.

6.3 Measurement setup

The goal of the measurements, and also this thesis, is to study the effect of the TL-cloak shown in Figure 30 on the antenna blockage caused by the reference object shown in Figure 31. The antenna blockage, in this context, means the amount of distortion to the radiation pattern of the AUT caused by the obstruction. Ideally, we would like to fully restore the antenna's radiation properties in a certain frequency band by cloaking the reference object using the TL-cloak. The antenna blockage is studied by measuring the H-plane radiation pattern of the AUT with the cloaked object and the bare reference object placed alternately in front of the AUT and by comparing these patterns to the radiation pattern of the AUT in free space.

The basic measurement setup used for the radiation pattern measurements is shown in Figure 33. The whole measurement is conducted inside an anechoic chamber, and the antennas are level. The measurement system works as follows. A signal with a certain frequency is transmitted by a HP 8722C vector network analyzer (VNA) (for frequencies 40 MHz – 40 GHz) and fed from port 1 of the VNA into the instrumentation antenna. Like is typical in a radiation pattern measurements, the static instrumentation antenna acts as a transmitter and the rotating AUT as a receiver. In this case, the signal received by the AUT is further amplified using a Minicircuits 15542 ZVE-8G amplifier before it is fed back to port 2 of the VNA. The VNA then combines the information of the transmitted and received power levels into a S_{21}-value. This measurement is repeated 360 times for different azimuthal rotation angles of the AUT and also for all the wanted frequencies. The measurement system is fully automated so that both the VNA and the Flam & Russell 8502 positioner programmer/controller are connected to a computer which is used to control the whole measurement setup. Both the frequency range and the wanted AUT azimuthal rotation angles are entered into the commercial antenna measurement software Orbit/FR FR959 Plus which then conducts the measurement. The measurement results are then further analyzed and saved to a text file using Orbit/FR DataPro software. Finally, this text file can be imported into MATLAB and the resulting radiation pattern plotted.

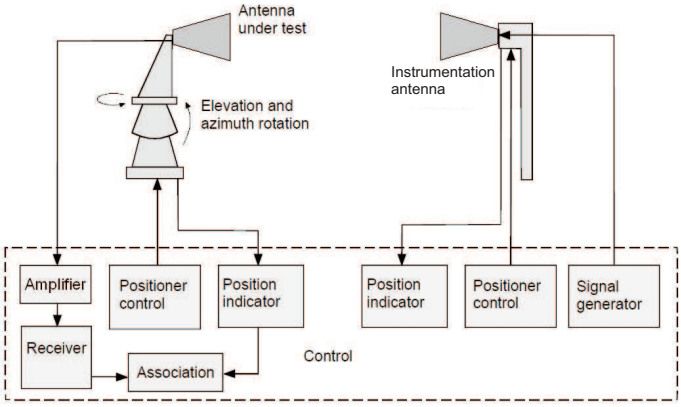

Figure 33: Basic measurement setup.

6.3.1 Anechoic chamber

The measurements are conducted in the large anechoic chamber of the Department of Radio Science and Engineering which has dimensions 6.3 m × 8.7 m × 5.5 m and uses polyurethane foam as the RF absorbing material. The anechoic chamber in question can be seen in Figure 34 with the dimensions of the chamber shown in Figure 35. The chamber is designed for frequencies 10 GHz and above. At these frequencies the reflectivity level is −35 dB or better. However, the reflectivity has also been measured for lower frequencies [53,54]. With two dipole-type of antennas, the reflectivity level was measured to be −15 dB at 900 MHZ and −21 dB at 1.88 GHz with uncertainties of ±3 dB at 900 MHz and ±1.5 dB at 1.88 GHz. Because we are using two directive antennas instead of dipoles and our operational frequency is 3 GHz, the reflectivity level can be expected to be much better than −21 dB though probably worse than −35 dB.

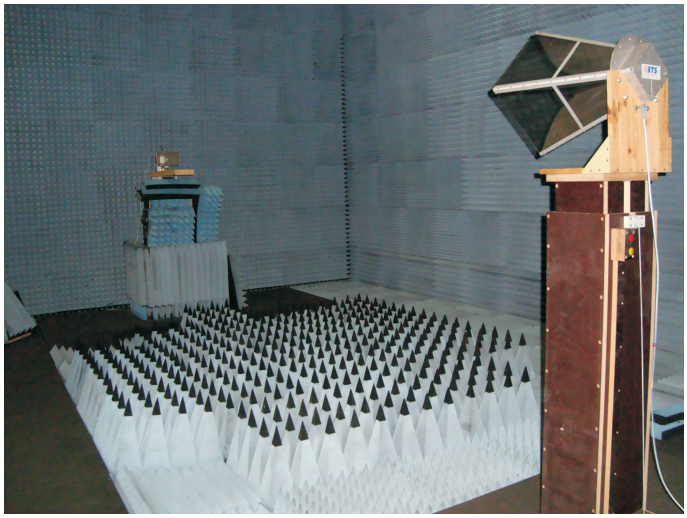

Figure 34: Anechoic chamber where the measurements were conducted with the reference horn antenna in the foreground and the measurement setup for the cloak in the back.

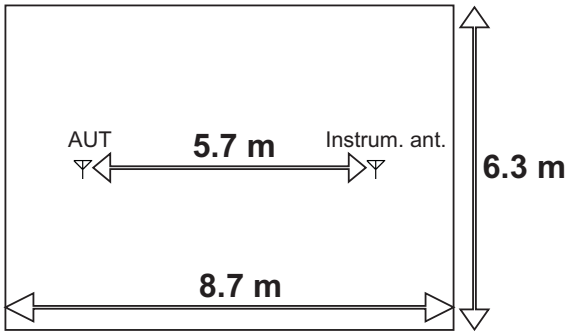

Figure 35: Dimensions of the anechoic chamber.

6.3.2 Antennas

Two antennas are needed in the measurements: the instrumentation antenna and the AUT. The instrumentation antenna used is EMCO diagonal dual-polarized horn antenna model 3164-03 designed for frequency range of 0.4 – 6 GHz. The antenna has two ports: one for horizontal and one for vertical polarization meaning that the antenna does not have to be rotated in order to change the polarization. The antenna stand is attached to a small 24 V motor which allows the antenna to be raised and lowered electronically. This was used to vertically align the antennas. The antenna and its stand can be seen in Figure 36(a). The antenna under test was Schwarzbeck BBHA 9210A double ridged wideband horn designed for the frequency range 0.7 – 5 GHz which can be seen in Figure 36(b).

Using equation (27), we can determine the far-field condition for the transmitting instrumentation antenna knowing that the antenna aperture is 33 cm × 33 cm. For the operational frequency 3 GHz, we get the far-field distance of about 2.18 m. As the distance between the antennas is 5.7 m, we can clearly conclude that the AUT is in the far field of the transmitting antenna as it should be in a radiation pattern measurement. In fact, the far-field condition is satisfied for all frequencies smaller than 7.85 GHz.

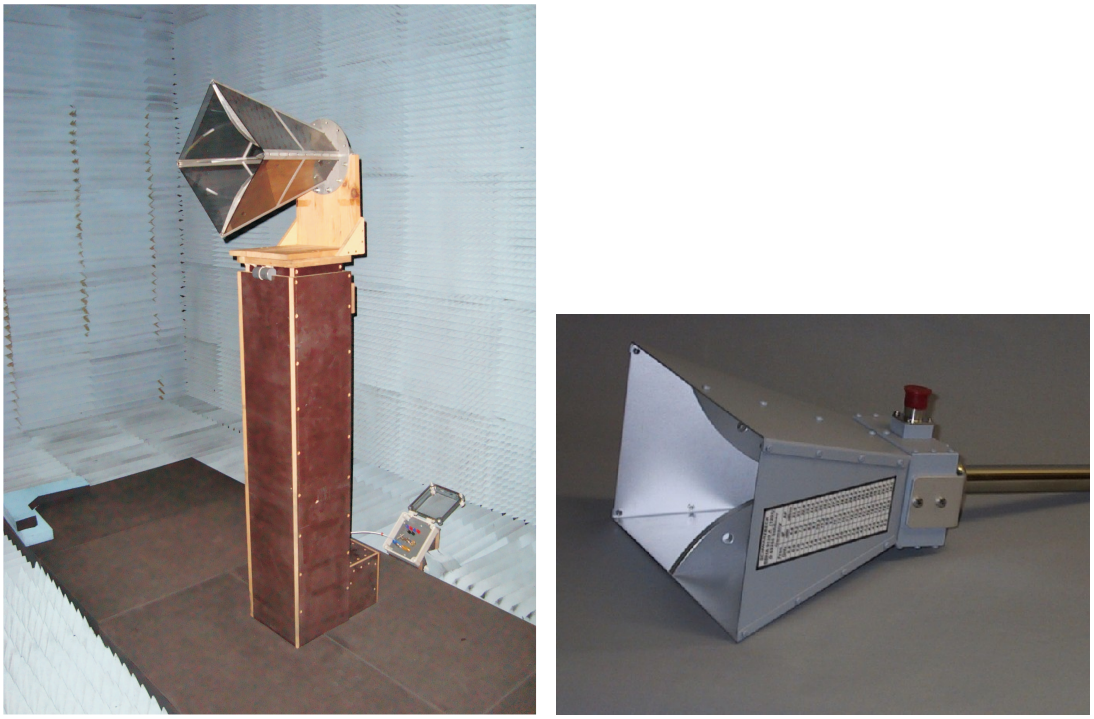

(a) (b)

Figure 36: Antennas used in the measurements: (a) the instrumentation antenna: EMCO 3164-03. (b) The antenna under test: Schwarzbeck BBHA 9210A [55].

6.3.3 Rotating stand for the cloaked object

Because now we want to measure not only the radiation pattern of the antenna but also the radiation pattern when there is an obstruction in front of the antenna, both the AUT and the cloaked or uncloaked object have to be rotated with the rotational axis being the rotational axis of the antenna. For this purpose, a measurement setup of Figure 37 where a wooden plank is attached to the rotating AUT was built. Also, below the plank a metal platform was added in order to raise the AUT and thus make it possible to align the two antennas vertically as otherwise the instrumentation antenna could not have been lowered to the AUT's level. A groove was milled to the wooden plank where the cloak is placed in order to make the cloak more stable during rotation and to help the alignment of the cloak. The setup allows movement of the AUT both vertically and horizontally, away or towards the object. The metal parts of the setup are covered during the measurements from transmitter direction with RF absorbing material as can be seen in Figure 37.

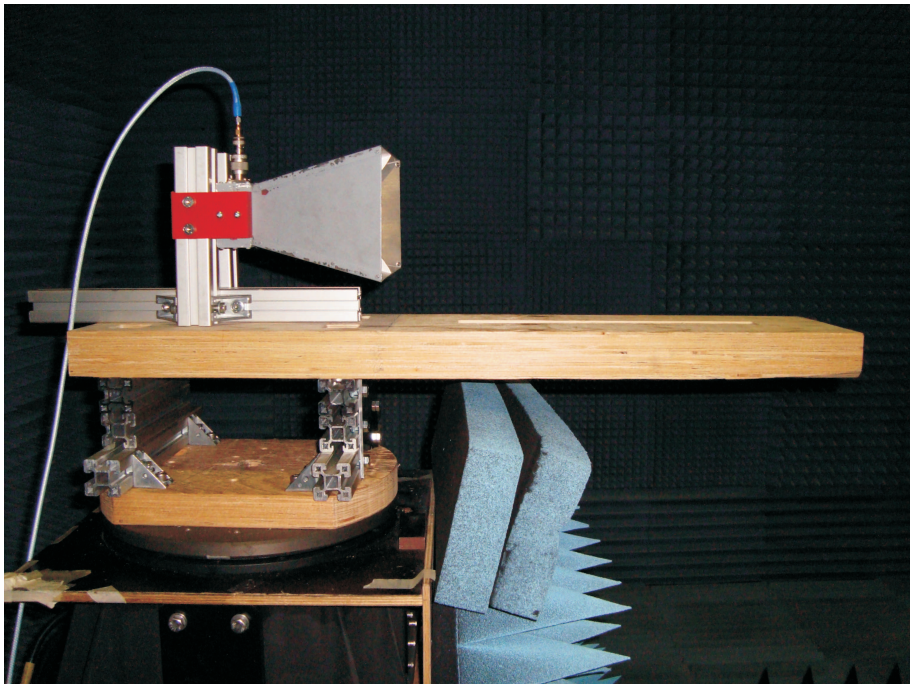

Figure 37: Rotating stand for the cloaked object.

6.4 Measurement scenarios

Several different measurement scenarios were devised in order to fully quantify the cloaking properties of the cloak. In the basic measurement case, the AUT is aligned, both vertically and horizontally, to point towards the middle of the cloak and the distance between the AUT and the cloak (or the object) center is 10 cm. The instrumentation antenna as well as the AUT use vertical polarization. The H-plane radiation pattern, i.e., the pattern with $\theta = 90^\circ$ and varying φ, is measured without the object or the cloak, with the cloaked object, and with just the bare, uncloaked object. The cloak is positioned so that the transmission lines of the network are either parallel or perpendicular to the direction of propagation. It should also be noted that the free-space pattern is measured using the setup of Figure 37, i.e., with the wooden plank attached to the antenna.

Several different variations of this measurement are conducted where in each some dimension of the basic setup is changed. In all the cases, the radiation pattern is measured for both the cloaked and the uncloaked object. Firstly, the distance between the AUT and the cloak center is varied from 10 cm to 20 cm, 30 cm and, finally, 40 cm. Secondly, the cloak is positioned horizontally 5 cm off the center of the AUT beam. As the cloak is no longer aligned along the groove on the wooden plank, the height of the antennas has to be adjusted slightly so that they are still pointing at the center of the cloak vertically. Thirdly, the cloak is raised 5 cm so that the antennas no longer point at the vertical center of the cloak. This measurement was conducted for the AUT–cloak center distances 10 cm and 30 cm. Fourthly, the cloak is rotated 45° in the horizontal plane so that the transmission lines of the network are diagonal to the direction of propagation.

6.5 Validation through simulations

In order to validate the measurement results, the first two and the last of the measurement scenarios described in Section 6.4 are replicated with commercial simulation software HFSS. Figure 38 shows the simulation model for the case where the center of the cloak is positioned 10 cm away from the antenna. The antenna in the simulations is modeled faithfully after the real Schwarzbeck BBHA 9210A measurement antenna and fed using a lumped port feed placed between the two vertical curving fins. The port creates a potential difference, i.e., a voltage, between the two fins, thus, exciting the antenna. Like in the earlier scattering simulations, symmetry boundaries are employed as a way of reducing computing time. In the yz-surface next to the cloak, the H-field symmetry boundary is used as the antenna was vertically polarized meaning that the created electric field is parallel to the z-axis, whereas in the bottom xy-surface E-field symmetry boundary is employed. The rest of the outer boundaries are assigned as radiation boundaries. After the simulation, the H-plane radiation pattern for each scenario is plotted using an intrinsic function of the software and compared to the corresponding measured pattern.

The measurement scenarios where the symmetry of the setup is broken by moving the cloak either horizontally or vertically are not simulated. In these simulations only one symmetry boundary could have been employed thus doubling the size of the model. This would in turn have made the simulation time very long.

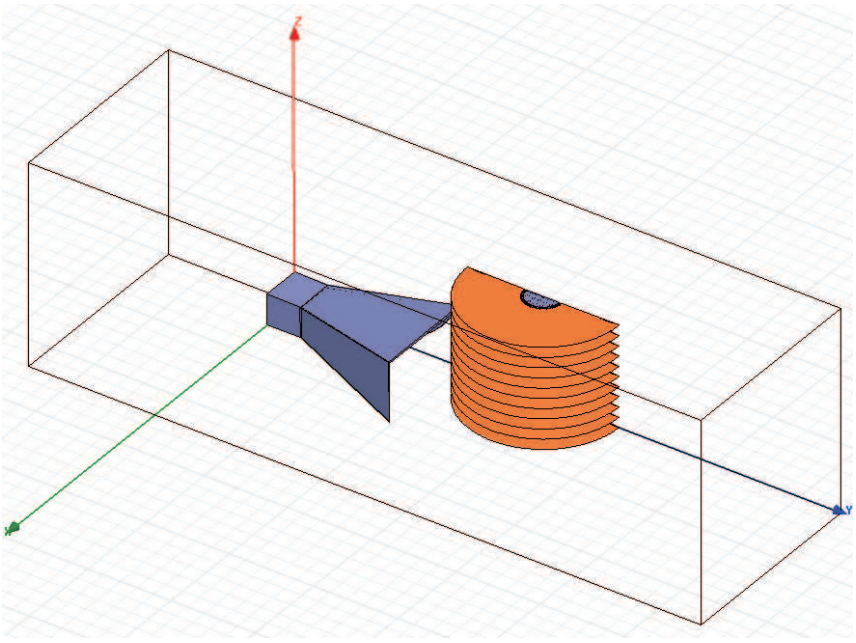

Figure 38: Simulation model for the case where the center of the cloak is positioned 10 cm away from the antenna.

7 Results

7.1 Antenna blockage

The measurement case where the distance between the AUT and the center of the cloak is 10 cm and the cloak is positioned in the center of the beam of the transmitting antenna both horizontally and vertically is considered here as the basic measurement scenario. Various dimensions of this basic setup are altered in later measurements, but this measurement is primarily used to validate the operation of the cloak. This particular setup was chosen as the basis because the object is almost as close to the AUT as it could be without the cloak touching the antenna. Thus, the bare reference object can be expected to scatter a large part of the radiation deforming the radiation pattern considerably. Therefore, this can be considered to be the most difficult scenario for cloaking.

Earlier during the design phase, the normalized total scattering width of the cloak was calculated using HFSS simulations (see Figure 23). Based on this, we know that the cloak should work best at the frequency of 3 GHz with the performance deteriorating as we move away from that frequency. However, as the cloaking is quite broadband, in frequencies close to 3 GHz, e.g., at 2.5 GHz and 3.5 GHz, we should still get reasonably good cloaking performance. The measured radiation patterns for the AUT in free space, with the cloaked object in front of it, and with the uncloaked object in front of it as well as the corresponding simulated patterns are plotted in Figures 39–41 with the solid lines denoting the measurement results and the dashed lines corresponding to simulations. The measured patterns for the cloaked and uncloaked object are normalized to the maximum of the measured free space pattern.

Clearly, it can be observed that the cloak works as intended not only at 3 GHz but also quite well at 2.5 GHz and 3.5 GHz. Furthermore, there is fairly good agreement between the measurements and the simulations, especially at 3 GHz. For example at 3 GHz and $\varphi = 0°$, the reference object without the cloak attenuates the received signal by approximately 6.5 dB according to the measurements. When the object is cloaked, the original free-space pattern is fully restored. The simulation results are similar though the minima and the maxima of the measured and simulated blocked main beams do not align which is the reason why the simulated attenuation at $\varphi = 0°$ is only 4.6 dB. There are, also, other small differences between the measured and simulated results. Notably at 2.5 GHz, there is a minimum at $\varphi = 0°$ in the measured patterns for the free space and cloaked object cases which cannot be seen in the simulations. Neither can it be seen in the free-space radiation pattern measured by the antenna manufacturer [56]. Therefore, it can be concluded that this deviation in the pattern is most likely caused by measurement errors or the measurement setup itself, e.g., reflections from the metal base or the attenuation by the wooden plank. Also, according to both simulations and measurements the cloak acts as a slightly directive element at 3.5 GHz as the maximum of both of these patterns is a bit larger than 0 dB.

Though the measured and simulated patterns coincide quite well, there are still

some noteworthy sources of error in the measurement. Probably the biggest source of error is the noticeable variation in the measured power level as a function of time. This was most likely due to the amplifier heating up considerably during the measurements thus affecting the available gain. As the measurement results are normalized to the free-space pattern, this has an effect on all of the measurement patterns. In order to prevent this excessive heating, the amplifier was turned off between measurements. Also, though the measurement setup was covered in RF absorbing material, some reflections from the metal base could still have reached the receiving antenna as, for example, just under the wooden plank there was a slight gap in the absorber coverage to allow the wooden plank to rotate freely as can be observed from Figure 37.

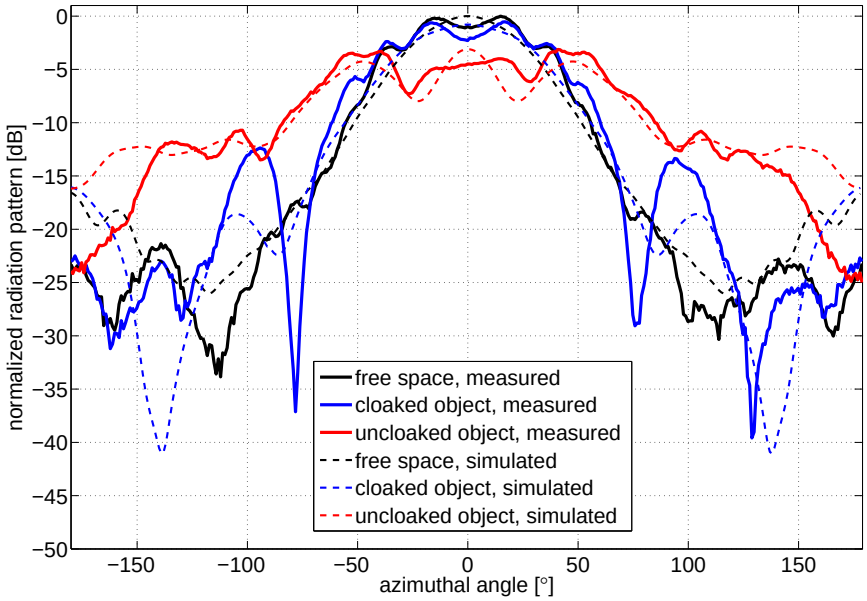

Figure 39: Radiation patterns when distance between the horn and the center of the reference object / cloak equals 10 cm and $f = 2.5$ GHz.

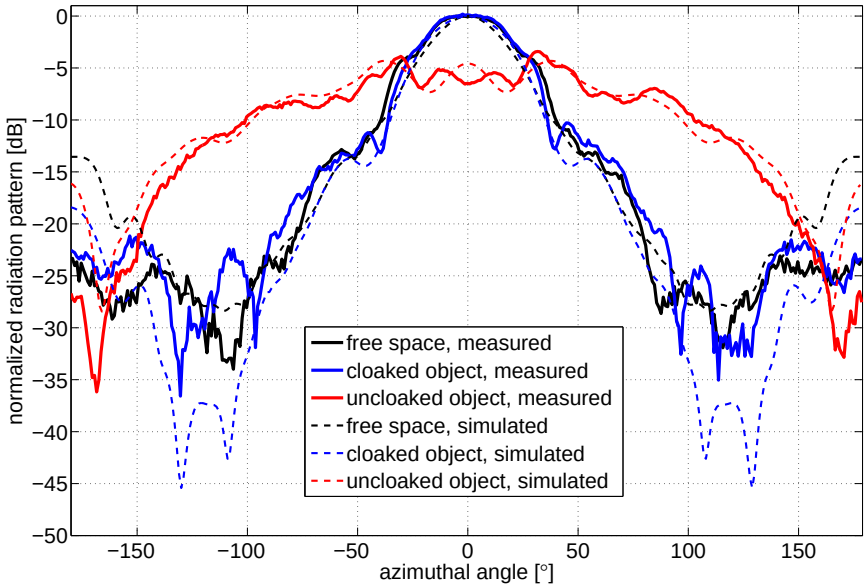

Figure 40: Radiation patterns when distance between the horn and the center of the reference object / cloak equals 10 cm and $f = 3.0$ GHz.

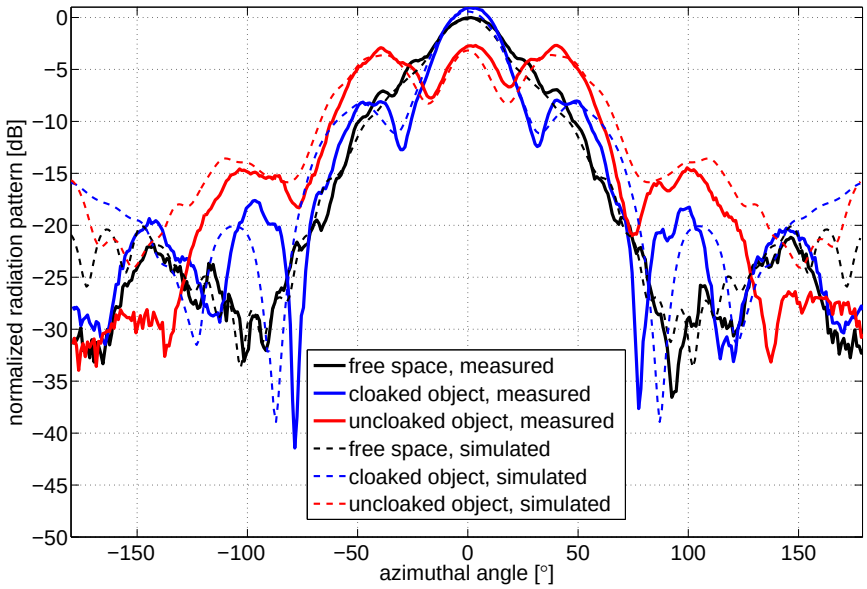

Figure 41: Radiation patterns when distance between the horn and the center of the reference object / cloak equals 10 cm and $f = 3.5$ GHz.

7.2 Changing the distance between the cloak and the antenna under test

In the next set of measurements, the distance between the AUT and the cloak center is varied between 20 cm, 30 cm, and 40 cm. As the size of the antenna aperture of the AUT is 245 cm × 142 cm, the far-field distance calculated according to (27) is about 1.2 m at 3 GHz. Therefore, the cloak is still clearly in the near field of the antenna in all the cases. For the limit between reactive and radiative near-field regions, equation (26) gives the distance of 23.8 cm. So, as we change the distance between the cloak and the antenna from 10 cm to 40 cm with the spacing of 10 cm, we are actually moving from the reactive near-field region to the radiative near-field region.

The measurement results for the AUT–cloak distances 20 cm, 30 cm and 40 cm for the frequency of 3 GHz are shown in Figures 42–44. Though not all of these results are as favorable as the ones presented in Section 7.1, especially when it comes to agreement between the measurements and the simulations, the cloak does clearly work as intended restoring the free-space radiation pattern in all the measured cases. Also, all the main features of the simulated curves are replicated in the measurement results. For example, the multiple side lobes visible in the simulated patterns for the reference object are replicated quite well in the measurement results though with a slight offset in the φ-angle. However, there are some small discrepancies, e.g., in Figure 42 there is a minimum in the measured main lobe for the cloaked case which cannot be seen in the simulations. Despite of this, it can be concluded that the operation of the cloak remains effectively the same as it is moved farther away from the AUT, at least when we are still reasonably close to the AUT, i.e., in the near field. Obviously, though there are no measurement results, we should also expect the cloak to work even when the distance between the AUT and cloak is much larger as the simulations of Section 5.1 show that the cloak scatters very little in the case of an incident plane wave.

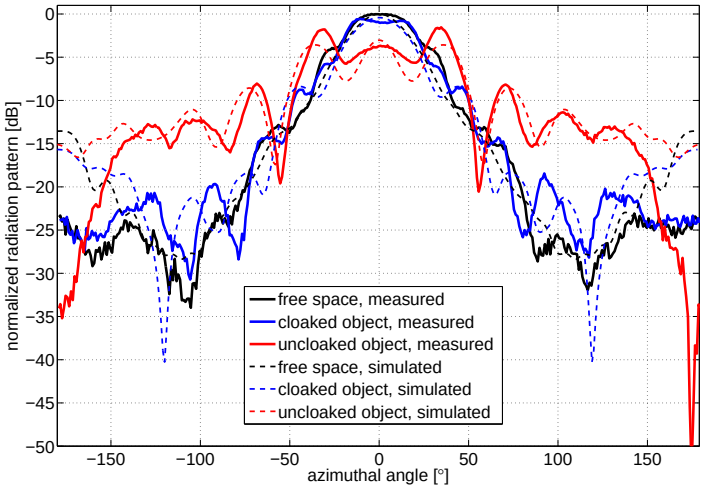

Figure 42: Radiation patterns when distance between the horn and the center of the reference object / cloak equals 20 cm and $f = 3.0$ GHz.

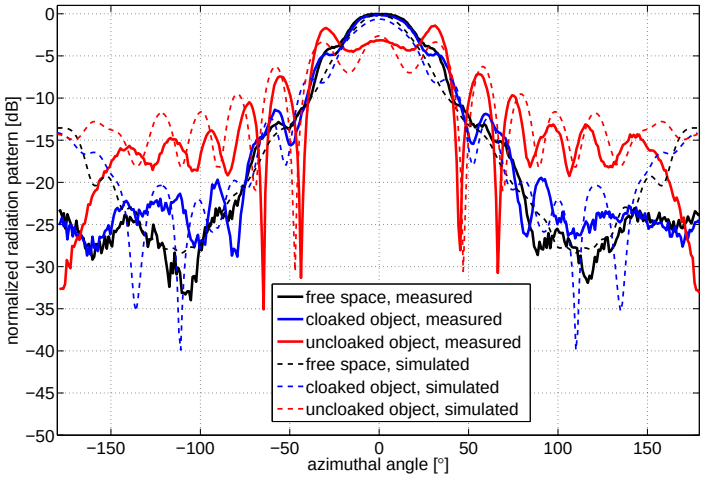

Figure 43: Radiation patterns when distance between the horn and the center of the reference object / cloak equals 30 cm and $f = 3.0$ GHz.

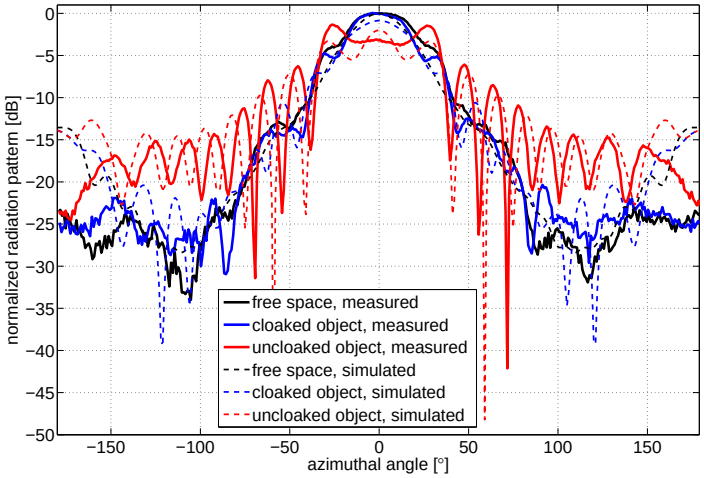

Figure 44: Radiation patterns when distance between the horn and the center of the reference object / cloak equals 40 cm and $f = 3.0$ GHz.

7.3 Cloak positioned 5 cm off center horizontally

Next, the cloak is positioned 5 cm off the center of the wooden plank with the distance along the antenna main radiation direction between the cloak center and AUT still being 10 cm, i.e., the center of the cloak is positioned at an angle of +26.6° off the antenna main radiation direction and 11.2 cm away from the AUT aperture center. The measured radiation pattern can be seen in Figure 45. In this case, unlike in earlier measurements, the radiation pattern is not fully restored. There is some noticeable asymmetry in the radiation pattern also for the cloaked object, i.e., some of the radiation is still scattered. For example at $\varphi = 56.5°$, the amplitude is 3.0 dB down compared to the free space pattern where as at $\varphi = -56.5°$ the amplitude is 2.6 dB up compared to the free space pattern. Furthermore, the clear peak visible in the pattern for the uncloaked object near $\varphi = -26.6°$, where a large part of the radiation hitting the object is reflected to the AUT, can be seen, though greatly reduced, also in the pattern for the cloaked object. However at angles closer to 0°, the agreement between the free-space pattern and the asymmetric cloak pattern is still very good and at all angles the improvement is considerable compared to the uncloaked case.

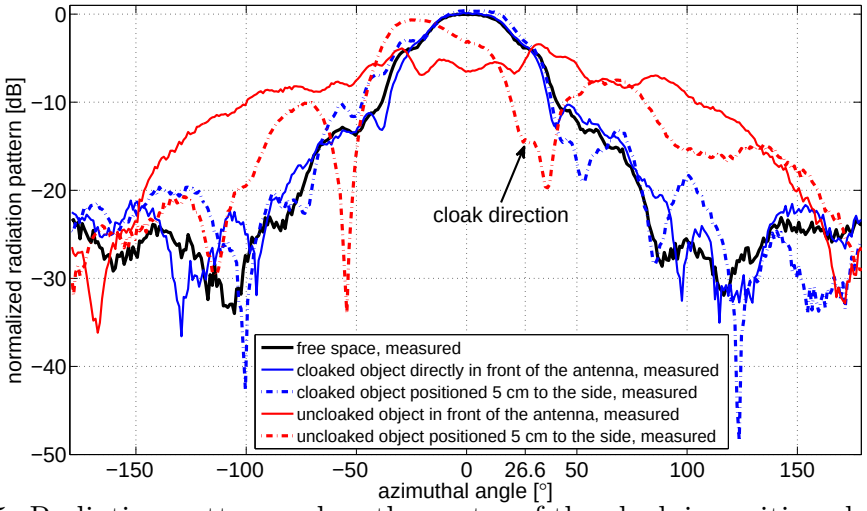

Figure 45: Radiation patterns when the center of the cloak is positioned at an angle of +26.6° off the antenna main radiation direction and 11.2 cm away from the AUT aperture center and $f = 3.0$ GHz.

7.4 Cloak positioned 5 cm off center vertically

In this measurement both of the antennas are raised 5 cm which corresponds to moving the cloak 5 cm vertically. The measured radiation patterns for the frequency of 3 GHz are shown in Figures 46 and 47. As can be observed, the cloak still performs well in these conditions. Noticeably, the reference object scatters more now compared to the case where the reference object was centered vertically. This is probably due to increased scattering from the corners of the object. Otherwise, Figures 46 and 47 are fairly close to Figures 40 and 43 which show the corresponding measurement results with the cloak positioned in the vertical center.

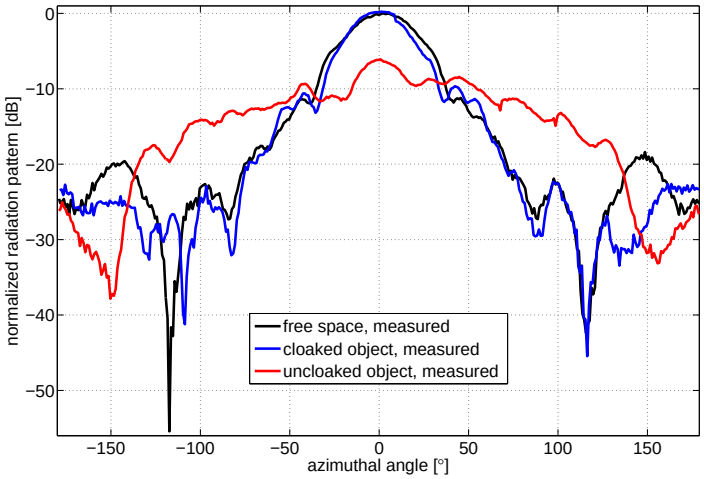

Figure 46: Radiation patterns when distance between the horn and the center of the reference object / cloak equals 10 cm, $f = 3.0$ GHz and the cloak is lowered by 5 cm.

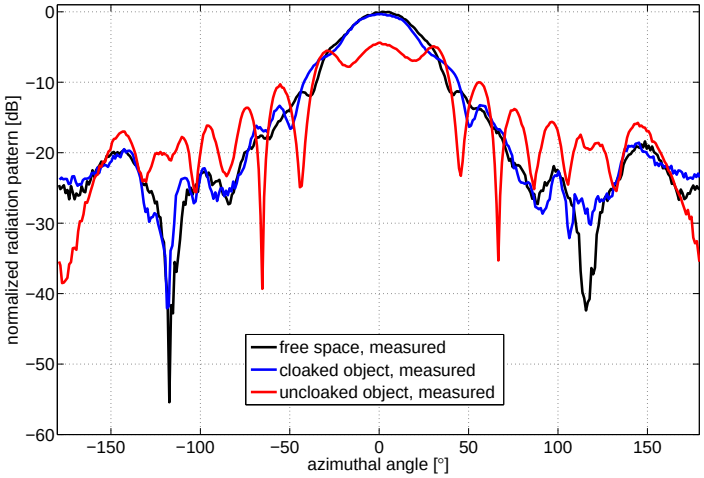

Figure 47: Radiation patterns when distance between the horn and the center of the reference object / cloak equals 30 cm, $f = 3.0$ GHz and the cloak is lowered by 5 cm.

7.5 Cloak rotated 45°

In Section 4.2, it was shown that the propagation inside the TL network should be similar no matter how the network is rotated in relation to the incident wave as long as the product $k_{\mathrm{TL}}d$ is suitably small where k_{TL} is the propagation constant inside the transmission line and d is the period of the TL network. As the transmission lines are effectively air-filled, we have for the operational frequency of 3 GHz $k_{\mathrm{TL}}d = k_0 d = \frac{2\pi f}{c} d \approx 0.44$. With the value $x = \sqrt{2} \times 0.44$, the second and third terms of the series of (46) equal to 0.1934 and 0.0062, i.e., the contribution of the third term and the higher order terms can be considered "small" and the approximate formula (47) is valid. Therefore, as the transition layer also has circular symmetry, the cloak should also work similarly regardless of how the cloak is rotated with the rotational axis being along the metal rods. In order to verify this, the cloak was rotated 45° so that the transmission lines are diagonal, not parallel/perpendicular as before, relative to the propagation direction and the measurement of Section 7.1 was repeated. The measured and simulated radiation patterns for the cloaked object can be seen in Figure 48. Both the measured and simulated results show that rotating the cloak does not affect the cloaking performance considerably at 3 GHz, as expected.

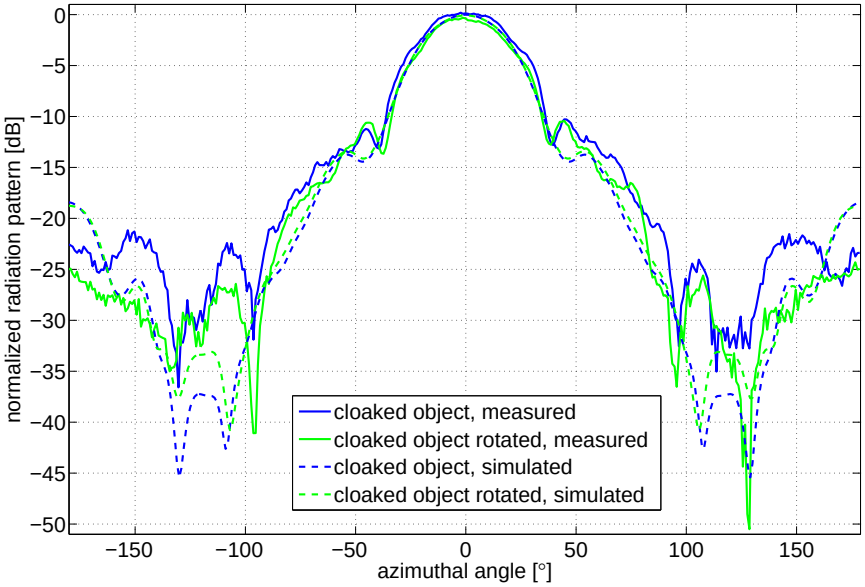

Figure 48: Radiation patterns when distance between the horn and the center of the reference object / cloak equals 10 cm and $f = 3.0$ GHz.

8 Transmission-line cloak used as an antenna

During the simulations of the TL-cloak, the idea arose that the same cloak structure could perhaps be used as an antenna at a frequency lower than the operational frequency of the cloak while still retaining the cloaking properties of the structure. This would allow us, for example, to position several antennas of different frequencies very close to each other without having to worry about mutual coupling between them. By joining the outermost cloaked metal cylinders to the corresponding transition layer metal cones and feeding the structure from the middle, the manufactured TL-cloak would essentially form a dipole-type antenna. But how do the other metal cones affect the radiation properties of the antenna and does the structure still with these modifications work as a cloak in the higher frequencies?

This concept of the TL-cloak acting as an antenna is verified by simulating the structure using Ansys HFSS software. Like mentioned before, two alterations are made to the basic cloak geometry shown in Figure 22 and the dimensions specified in Table 1 in order to create a dipole-like antenna. Firstly, the radius of the outermost reference object metal cylinders is increased from 19.5 mm to 22 mm so that there is a connection between them and the corresponding transition layer metal cones. Secondly, a vertical gap is made to the middle metal cylinder, and the structure is fed from that gap using a lumped port feed. These two alterations are shown in Figure 49.

Two simulations are needed in order to fully verify the operation: one to see that the cloak still works as a cloak in the higher frequencies despite of the modifications made to the geometry and one to see if the cloak works as an antenna in a lower frequency range. In the first simulation, the structure is illuminated with a plane wave and the normalized total scattering width is attained from the simulation results, similar to earlier simulations in Section 5.1. For the frequency of 3 GHz, the ratio of the normalized total scattering width is calculated to be 0.066 which is very close to the value that can be read from Figure 23 for the original cloak. In the second simulation, the structure is fed with a lumped port feed as shown in Figure 49(b) and the S_{11} for that port, which tells how much of the power fed to the antenna is reflected back, is calculated over quite a wide frequency range of 50 – 900 MHz. After that the fields are solved for the found resonance frequencies. The simulated S_{11} for the lumped port can be seen in Figure 50. In the frequency range 50 – 900 MHz, there are two resonances: at 302 MHz and 684 MHz. The two simulated directivity patterns corresponding to these two resonances can be seen in Figure 51. The lowest resonance exhibits a nice dipole-like radiation pattern whereas the higher mode has a more complex radiation pattern. Also, the current distribution at 302 MHz, shown in Figure 52(a), corresponds to the current distribution of a half-wave dipole, shown in Figure 52(b). While the complicated pattern of the higher resonance makes it quite hard to use in any real application, the lower (or in fact the lowest) resonance exhibits many advantageous antenna properties.

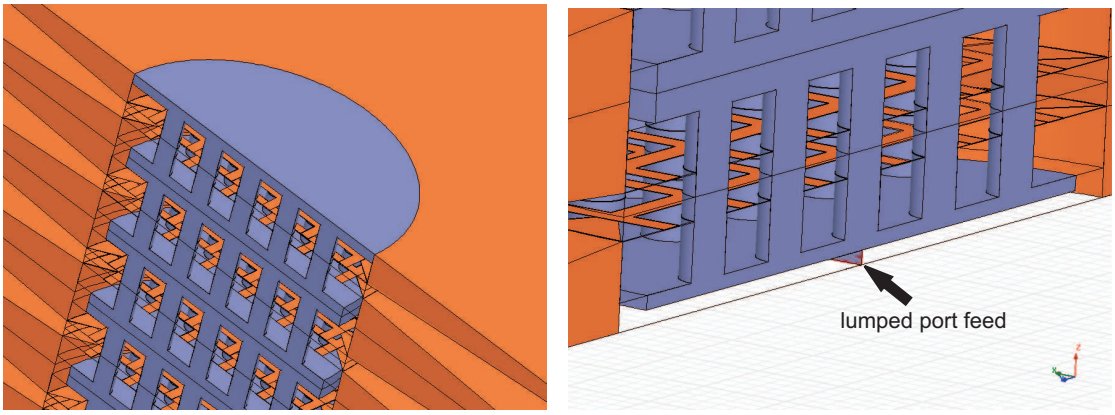

(a) (b)

Figure 49: Two modifications to the basic cloak geometry: (a) the radius of the outermost metal cylinders is increased so that they are connected to the corresponding transition layer metal cones; (b) a lumped port feed is placed in the center of the middle metal cylinder.

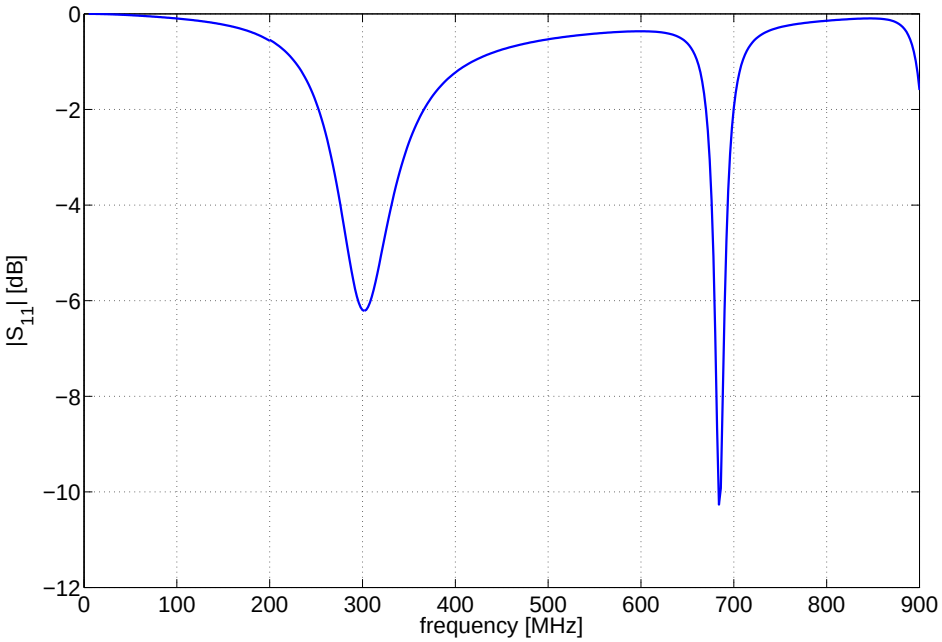

Figure 50: $|S_{11}|$ for the lumped port feed of the cloak-antenna.

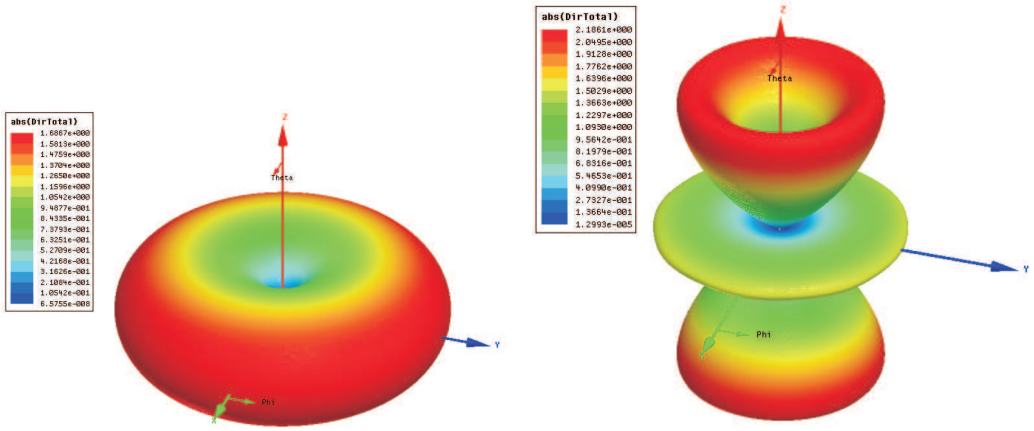

(a) (b)

Figure 51: Directivity patterns for the two lowest resonance modes: (a) the lowest resonance at 302 MHz; (b) the second lowest resonance at 684 MHz.

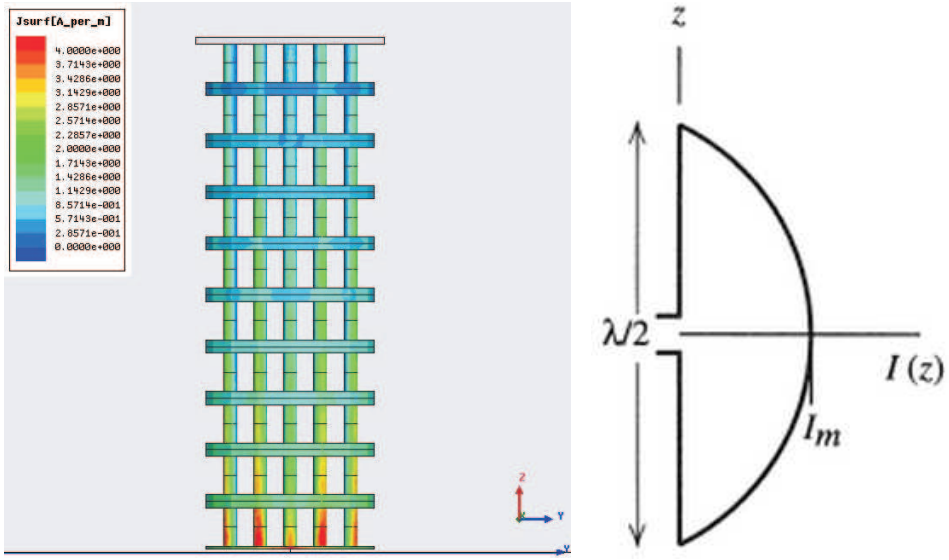

(a) (b)

Figure 52: (a) Surface currents on the cloaked reference object at the frequency of 302 MHz when the structure is fed with a lumped feed (Only half of the reference object is shown as symmetry boundaries are used in the simulation and the cloak itself is rendered invisible for clarity);(b) The current distribution of a half-wave dipole antenna [57].

It would be useful if we could somehow tune the two frequencies, the cloaking frequency and the antenna resonance frequency, independently. It was described in Section 5.1 how the the cloaking frequency can be tuned by scaling the whole structure relative to the wavelength. Once this is done, the tuning of the antenna resonance frequency should be done so that there is no shift in the cloaking frequency. The resonance frequency of this type of an antenna f_r is defined as

$$f_r = \frac{1}{2\pi}\frac{1}{\sqrt{LC}}, \tag{50}$$

where L is the inductance, which in this case arises from the current flowing along the reference object between the outermost metal cones, and C is the capacitance, which in this case comes from the capacitance between the outermost metal cones. According to (50), increase in the capacitance clearly results in lowered resonance frequency. By inserting a thin metal disc on both ends of the cloak-antenna and changing the radius of these discs, the total capacitance of the antenna can be varied. The discs effectively form an air-filled parallel plate capacitor which has capacitance

$$C = \frac{\epsilon_0 A}{h}, \tag{51}$$

where A is the area of a parallel plate and h is the separation between the top and bottom plates. Most importantly, the capacitance is directly proportional to the area of a single parallel plate or to the square of the radius of the discs. If we assume that the capacitance of the cloak-antenna has the form of (51) and insert (51) into (50), we can see that the resonance frequency is inversely proportional to the radius of the discs. Obviously, this is only a crude estimation of the capacitance of the structure. It does not take into account, e.g., the metal cones between the metal discs. The true physics of the structure are more complicated.

The behavior of the resonance frequency as the radius of the metal discs changes is, again, verified using HFSS simulations. A parametric sweep varying the radius of the metal discs from 90 mm, i.e., the same size as the metal cones, to 190 mm is employed. The metal discs are 0.5 mm thick. The resulting S_{11}-curves for the lumped port feed can be seen in Figure 53. Clearly as we increase the radius, the resonances drop to lower frequencies. Also at the same time, the first resonance sharpens and the bandwidth of the resonance gets narrower. By increasing the radius of the metal discs by 100 mm, the resonance frequency is made to drop by more than 100 MHz, from 302 MHz to 197 MHz. The resonance frequency could be dropped even further down by further increasing the size of the discs though making the discs much larger is not very practical. It should be noted that the resonance frequency is not in fact exactly inversely proportional to the radius of the discs as was presumed before. This was to be expected as (51) is only a crude estimation of the capacitance of the structure.

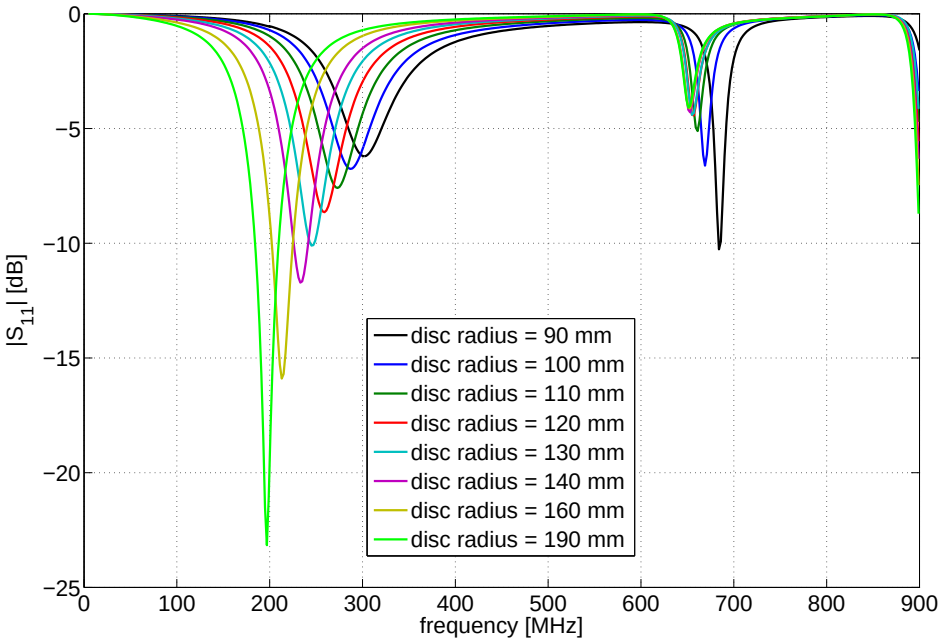

Figure 53: $|S_{11}|$ for the lumped port feed of the cloak-antenna when the radii of the metal discs on both ends of the structure is varied from 90 mm (the same size as the metal cones) to 190 mm.

Though the dipole-like cloak-antenna introduced earlier does clearly work as intended providing both the wanted cloaking and antenna properties, it is quite difficult to realize in practice, especially when it comes to feeding the structure. Furthermore, the existing manufactured cloak cannot be directly used for this design without breaking the structure. However, there is another way to use the cloak as an antenna which allows us to utilize the realized TL-cloak without breaking it. Instead of realizing a dipole-like antenna, the cloak could be converted into a monopole-like antenna by placing it on top of a metal ground plane and connecting the top metal cylinder to the corresponding transition layer metal cone. Now, the structure is fed between the ground plane and the bottom reference object metal cylinder. Because of the influence of the ground plane, the height of the structure is effectively doubled. This also means that the wanted antenna resonance frequency should be about half of the resonance frequency for the dipole-like antenna structure.

This idea is verified using HFSS simulations. The simulation method is the same as before with the aforementioned changes made to the geometry. However, now the simulations are conducted for an infinite ground plane and instead of an ideal lumped port feed, a 50 Ω coaxial feed is used. Figure 54 shows the simulated S_{11} for the monopole-like structure. It can be observed that the structure has its lowest resonance at 208 MHz which is somewhat higher than what we would expect, i.e., half of the resonance frequency for the dipole-like structure. This is probably due to decreased capacitance of the structure as the outermost metal cones are now farther away from each other than before. The directivity pattern for 208 MHz can be seen in Figure 55. As can be expected, the directivity pattern closely resembles that of a

monopole antenna. While the operation of the monopole structure as a cloak is not verified numerically due to very long expected simulation time, the structure can be expected to retain its cloaking ability despite of the modifications as the basic geometry of the structure is the same as in the case of the dipole-like structure with only the effective height of the cloak changing.

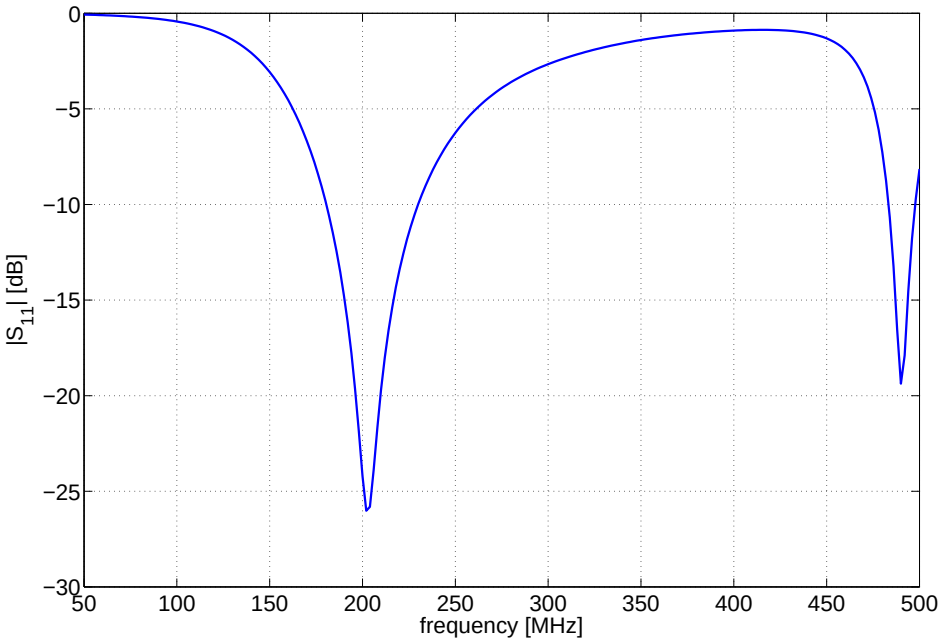

Figure 54: $|S_{11}|$ for the coaxial feed of the monopole cloak-antenna.

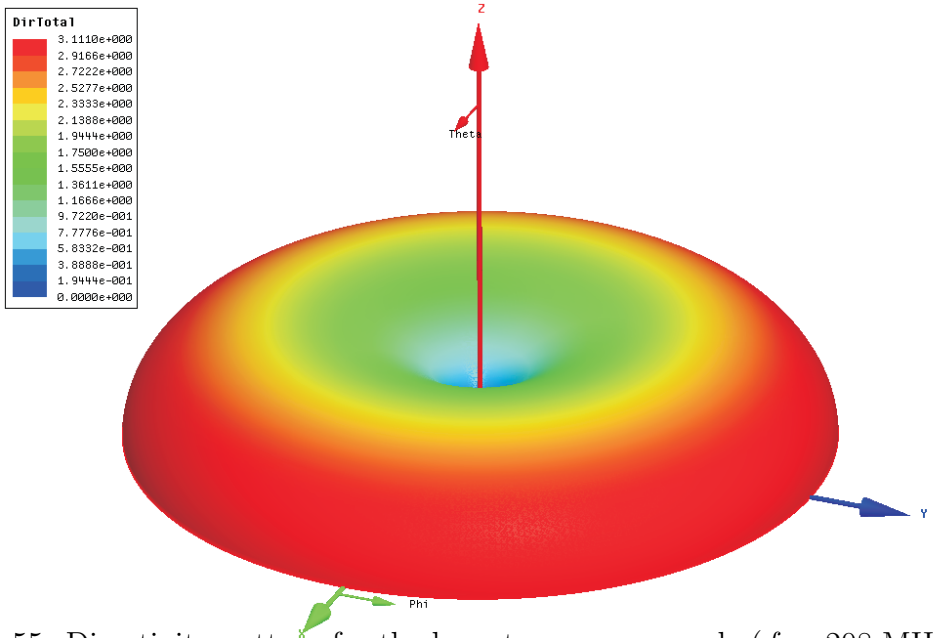

Figure 55: Directivity pattern for the lowest resonance mode ($f = 208$ MHz) of the monopole-like structure.

9 Future work

Though several papers, a dissertation and now this thesis have been written about TL-based cloaking, there is still a lot to be done. In the following, some improvements for the future cloak designs and further research directions are presented.

Though some attention was given to the overall weight of the cloak, the cloak is still quite heavy for practical use. One layer of the cloak weighs about 319.6 g. As there are 20 of these layers, the whole cloak weighs about 6.4 kg. One way to make the cloak lighter would be to make the transition layer cones out of some light non-metallic material, e.g., some hard plastic, which would then be coated with metal. In principle, the middle of the metal cones could also alternatively be hollow though such a structure could be quite difficult to manufacture. Making the cloak lighter would not only make it easier to handle, it would also alleviate the stress to the solderings between the metal cones and the PCB which can break fairly easily.

In this thesis, the total scattering of the cloak was simulated, but no measurements were done on the topic. In principle, the scattering cross section measurement could be done simply by positioning the cloak between the two antennas used in our measurements, in the far field of the antennas, and measuring S_{21} which corresponds to the total received field. The scattered fields could be attained from this by repeating the measurement, this time without the cloak, and subtracting the latter value from the former. Now, the scattering cross section, or alternatively the scattering width assuming that the cloak is sufficiently tall compared to the antenna beamwidth, for this particular scattering angle could be determined. However, in order to measure the total scattering, the S_{21} measurement should be repeated for several different scattering angles, i.e., receiving antenna positions, making the measurement quite laborious. Even bigger problem with the measurement is that the cloak itself is designed to scatter very little of the incident wave. Thus, we would need very sensitive equipment and an anechoic chamber with very low reflectivity in order to do the measurements well and get meaningful results.

Even with the basic setup used in the measurements of this thesis, several interesting measurements could still be done. One interesting property of the cloak that was not studied in this thesis is how the cloak works when it is tilted either towards the AUT or away from the AUT or sideways. In practical applications, the cloak may not always be perfectly aligned with the antennas. Therefore, it would be beneficial to know how sensitive the cloak is to this type of imperfection in the setup though the fairly heavy weight of the cloak makes this measurement somewhat difficult in practice.

The nature of this thesis was mainly experimental. However, there is also a lot of analytical work to be done on the topic. One important question that could be tackled using analytical means is, why the transition layer consisting of a set of gradually widening strips behaves differently from the transition layer consisting of a set of solid conical metal layers when the length of the transition layer is changed. In [45], it was shown that in the former case increasing the thickness of the transition layer caused the operational frequency to shift down where as in the latter case there is no shift in the operational frequency as was shown in Section 5.1. Clearly, there is

a fundamental difference in the way these two transition layers match the free space wave to the transmission line.

In this thesis, the idea of using the cloak as an antenna was only briefly introduced and only some tentative simulation results were presented. The logical next step would be to test the concept experimentally. The existing cloak could be used for this purpose without breaking it using the monopole antenna structure, i.e., by placing it on a large metal ground plane and feeding it from a gap between the outermost metal cylinder and the ground plane. Now, the 20-layer TL-cloak would essentially act as 40-layer TL-cloak due to the metal ground plane.

10 Summary

In this thesis, a novel TL-based electromagnetic cloak was designed and manufactured. The operational frequency of the cloak is 3 GHz. The design is based on earlier TL-cloak designs with two modifications to the basic cloak geometry: the transition layer which consisted of a set of gradually widening strips in the earlier studies was replaced with a set of solid conical metal layers and the transmission line networks were printed on a substrate layer as opposed to using separate grids of metal strips. The idea behind these changes was to make the new cloak more practical, simpler and easier to manufacture than the earlier manufactured cloaks. The optimal dimensions for the cloak were determined using computer simulations, more specifically Ansys HFSS software. A series of simulations with varying cloak dimensions was conducted where the cloaked object and the uncloaked object were separately illuminated with a plane wave, and based on the results the calculated scattering the normalized total scattering width of the cloak was determined for each case. The final cloak design was shown to scatter very little of the incident plane wave and have fairly wide bandwidth of operation. Furthermore, it was observed that the new transition layer design has markedly different behavior compared to the one based on a set of gradually widening strips: as the transition layer thickness is increased, the cloaking effect is more pronounced, but there is no shift in the operational frequency, unlike in the case of gradually widening strips.

It was shown numerically and experimentally that the designed TL-cloak is capable of hiding a mesh-like metal object placed inside it from the incident wave. More specifically, a scenario where the object to be cloaked was placed in the near field of a horn antenna was studied by conducting radiation pattern measurements in an anechoic chamber. Though several TL-cloak measurements have been conducted earlier inside a waveguide of some sort, the first results for a true free-space measurement of a transmission-line cloak were introduced in this thesis. It was shown that the free-space radiation pattern of a horn antenna can be restored by cloaking the object causing the deformation using the designed cloaking structure in a variety of different scenarios. The cloaking performance is not considerably hindered by moving the object closer or farther away from the antenna, by moving it vertically, by rotating it or by positioning it horizontally off-center though in the latter case the radiation pattern was slightly asymmetric even with cloaking. Also, good agreement between the measured and corresponding simulated results was achieved in all the cases, and the cloak was shown to work not only at the design frequency of 3 GHz but also reasonably well at a fairly wide bandwidth surrounding it.

The idea of using the TL-cloak as an antenna in the lower frequencies than the cloaking frequency was introduced. Two modifications to the cloak geometry are done in order to achieve this: the outermost metal cylinders of the reference object are connected to the corresponding transition layer metal cones and a gap is made to the middle metal cylinder and the structure is fed from the gap using a lumped port feed. It was shown using HFSS simulations that the new structure works effectively as an antenna at 302 MHz with a dipole-like donut-shaped radiation pattern while still working as a cloak at 3 GHz. A higher order resonance was also observed at

684 MHz with a more complex radiation pattern. Also, it was shown that by placing a thin metal disc on the top and bottom of the structure and varying its radius, the resonance frequency could be tuned. As the radius of the disc is increased, the capacitance of the structure also increases which means that the resonance frequency is decreased. Alternatively, the cloak could also be used as a monopole-like antenna by placing it on a large metal ground plane, feeding it between the ground plane and the bottom metal cylinder of the reference object and connecting the top metal cylinder to the corresponding transition layer metal cone. This would be much easier to implement in practice than the aforementioned dipole-like solution as the existing cloak would not have to be broken and the feeding the structure would be simpler. It was shown that also this structure can work simultaneously as an antenna in the lower frequencies and as a cloak in the higher frequencies. However, now due to the ground plane the length of the structure is effectively doubled causing the antenna resonance frequency to shift further down compared to the dipole case.

References

[1] A. Sihvola. "Metamaterials in electromagnetics." *Metamat.*, vol. 1, no. 1, pp. 2–11, Feb. 2007.

[2] A. Alù and N. Engheta. "Achieving transparency with plasmonic and metamaterial coatings." *Phys. Rev. E*, vol. 72, p. 016623, Jul. 2005.

[3] U. Leonhardt. "Optical conformal mapping." *Science*, vol. 312, pp. 1777–1780, Jun. 2006.

[4] J.B. Pendry, D. Schurig, and D.R. Smith. "Controlling electromagnetic fields." *Science*, vol. 312, pp. 1780–1782, May 2006.

[5] P. Alitalo, O. Luukkonen, L. Jylhä, J. Venermo, and S. Tretyakov. "Transmission-line networks cloaking objects from electromagnetic fields." *IEEE Trans. Antennas Propag.*, vol. 56, no. 2, pp. 416–424, 2008.

[6] P. Alitalo, S. Ranvier, J. Vehmas, and S.A. Tretyakov. "Microwave transmission-line network guiding electromagnetic fields through a dense array of metallic objects." *Metamat.*, vol. 2, no. 4, pp. 206–212, Feb. 2008.

[7] P. Alitalo, F. Bongard, J.-F. Zürcher, J. Mosig, and S. Tretyakov. "Experimental verification of broadband cloaking using a volumetric cloaking composed of periodically stacked cylindrical transmission-line networks." *Appl. Phys. Lett.*, vol. 94, no. 1, p. 014103, Jan. 2009.

[8] P. Alitalo, O. Luukkonen, F. Bongard, J.-F. Zürcher, J.R. Mosig, and S.A. Tretyakov. "Broadband cloaking of selected objects in the microwave regime with a volumetric cloak comprising layered networks of transmission lines," in *Proc. IEEE ISAP*, 2009, p. 222.2.

[9] L. Tähtinen. "Olisinpa näkymätön." *Tiede*, no. 6, 2007 (in Finnish).

[10] K. Chang. "Light fantastic: flirting with invisibility." *The New York Times*, June 12, 2007.

[11] V. Podlozny. "Virtual Institute for Artificial Electromagnetic Materials and Metamaterials METAMORPHOSE VI AISBL - Metamaterial definition." Internet: `http://metamorphose-vi.org/index.php?option=com_content&task=view&id=46&Itemid=70`, [Dec. 20, 2010].

[12] C. Caloz and T. Itoh. *Electromagnetic metamaterials: transmission line theory and microwave Applications.* USA, John Wiley & Sons, 2006, pp. 1–2.

[13] A. Alù and N. Engheta. "Plasmonic materials in transparency and cloaking problems: mechanism, robustness, and physical insights." *Opt. Express*, vol. 15, pp. 3318–3332, Mar. 2007.

[14] M.G. Silveirinha, A. Alù and N. Engheta. "Infrared and optical invisibility cloak with plasmonic implants based on scattering cancellation." *Phys. Rev. E*, vol. 75, p. 075107, Aug. 2007.

[15] A. Alù and N. Engheta. "Multi-frequency optical invisibility cloaks with layered plasmonic shells." *Phys. Rev. Lett.*, vol. 100, p. 113901, Mar. 2008.

[16] A. Alù and N. Engheta. "Plasmonic and metamaterial cloaking: physical mechanisms and potentials." *J. Opt. A*, vol. 10, p. 093002, Sep. 2008.

[17] A. Tricarico, F. Bilotti, A. Alù, and L. Vegni. "Design of plasmonic covers to cloak arbitrarily-shaped objects," in *Proc. Metamaterials 2009*, 2009, pp. 411–413.

[18] D. Schurig, J.J. Mock, B.J. Justice, S.A. Cummer, J.B. Pendry, A.F. Starr, and D.R. Smith. "Metamaterial electromagnetic cloak at microwave frequencies." *Science*, vol. 314, pp. 977–980, Nov. 2006.

[19] J. Valentine, J. Li, T. Zentgraf, G. Bartal, and X. Zhang. "An optical cloak made of dielectrics." *Nature Mater.*, vol. 8, pp. 568–571, Jul. 2009.

[20] J. Li and J.B. Pendry. "Hiding under the carpet: a new strategy for cloaking." *Phys. Rev. Lett.*, vol. 101, p. 203901, Nov. 2008.

[21] B. Zhang, Y. Luo, X. Liu, and G. Barbastathis. "Macroscopic invisibility cloak for visible light." *Phys. Rev. Lett.*, vol. 106, p. 033901, Jan. 2011.

[22] G.W. Milton and N.A. Nicorovici. "On the cloaking effects associated with anomalous localized resonance." *Proc. R. Soc. Lond. A: Math. Phys. Sci.*, vol. 462, pp. 3027–3059, Oct. 2006.

[23] N.A. Nicorovici, G.W. Milton, R.C. McPhedran, and L.C. Botten. "Quasistatic cloaking of two-dimensional polarizable discrete systems by anomalous resonance." *Opt. Express*, vol. 15, pp. 6314–6323, May 2007.

[24] A. Räisänen and A. Lehto. *Radiotekniikan perusteet.* Finland, Otatieto, 2003, pp. 81–84 (in Finnish).

[25] D.M. Pozar. *Microwave engineering.* USA, John Wiley & Sons, 2005, pp. 174–175.

[26] D.M. Pozar. *Microwave engineering.* USA, John Wiley & Sons, 2005, pp. 50–52.

[27] R.E. Collin. *Field theory of guided waves, 2nd ed..* USA, John Wiley & Sons, 1991, pp. 605–608.

[28] P. Alitalo. "Microwave transmission-line networks for backward-wave media and reduction of scattering." Doctoral dissertation, Helsinki University of Technology, Espoo, Finland, 2009, pp. 34–35.

[29] D.M. Pozar. *Microwave engineering.* USA, John Wiley & Sons, 2005, pp. 371–376.

[30] C. Caloz and T. Itoh. *Electromagnetic metamaterials: transmission line theory and microwave applications.* USA, John Wiley & Sons, 2006, p. 85.

[31] C. Caloz and T. Itoh. *Electromagnetic metamaterials: transmission line theory and microwave applications.* USA, John Wiley & Sons, 2006, pp. 113–115.

[32] A. Räisänen and A. Lehto. *Radiotekniikan perusteet.* Finland, Otatieto, 2003, pp. 56–57 (in Finnish).

[33] IEEE Antenna Standards Committee. *IEEE standard – definitions of terms for antennas.* USA, The Institute of Electrical and Electronics Engineers, 1983.

[34] W.L. Stutzman and G.A. Thiele. *Antenna theory and design, 2nd ed..* USA, John Wiley & Sons, 1998, pp. 24–43.

[35] W.L. Stutzman and G.A. Thiele. *Antenna theory and design, 2nd ed..* USA, John Wiley & Sons, 1998, pp. 51–52.

[36] W.L. Stutzman and G.A. Thiele. *Antenna theory and design, 2nd ed..* USA, John Wiley & Sons, 1998, pp. 299–316.

[37] Homepage of Schwarzbeck Mess - Elektronik. Internet: `http://www.schwarzbeck.de/Bilder/9120d.jpg`, [Jul. 8 2011].

[38] G.E. Evans. *Antenna measurement techniques.* USA, Artech House, 1990, p. 223.

[39] P.-S. Kildal, A.A. Kishk, and A. Tengs. "Reduction of forward scattering from cylindrical objects using hard surfaces." *IEEE Trans. Antennas Propag.*, vol. 44, pp. 1509–1520, Nov. 1996.

[40] P. Alitalo and S. Tretyakov. "Electromagnetic cloaking with metamaterials." *Mater. Today*, vol.12, no. 3, 2009, pp. 22–29.

[41] P. Alitalo, S. Maslovski, and S. Tretyakov. "Three-dimensional isotropic perfect lens based on LC-loaded transmission lines." *J. Appl. Phys.*, vol. 99, p. 064912, Mar. 2006.

[42] P. Alitalo, O. Luukkonen, J.R. Mosig, and S.A. Tretyakov. "Broadband cloaking with volumetric structures composed of two-dimensional transmission-line networks." *Microw. Opt. Tech. Lett.*, vol. 51, pp. 1627–1631, Jul. 2009.

[43] Homepage of Rogers Corporation. Internet: `www.rogerscorp.com`, [Aug. 29, 2011].

[44] Homepage of Evonik Industries' Rohacell. Internet: `www.rohacell.com`, [Aug. 29, 2011].

[45] P. Alitalo and S.A. Tretyakov. "Broadband electromagnetic cloaking realized With transmission-line and waveguiding structures." *Proc. IEEE*, vol.99, pp. 1646–1659, Oct. 2011.

[46] Homepage of Ansys HFSS. Internet: `www.ansoft.com/products/hf/hfss/`, [Sep. 3, 2011].

[47] P. Alitalo, J. Vehmas, and S.A. Tretyakov. "Reduction of antenna blockage with a transmission-line cloak," in *Proc. EUCAP*, 2011, pp. 2546–2549.

[48] Homepage of Precia. Internet: `www.precia.fi`, [Sep. 3, 2011].

[49] Homepage of Prinel Piirilevy Oy. Internet: `www.prinel.fi`, [Sep. 3, 2011].

[50] Homepage of Pertik Oy. Internet: `www.pertik.fi`, [Sep. 3, 2011].

[51] S-26.3120 Radio engineering, laboratory course - course handout, Department of Radio Science and Engineering, Aalto University.

[52] W.L. Stutzman and G.A. Thiele. *Antenna theory and design, 2nd ed..* USA, John Wiley & Sons, 1998, pp. 409–415.

[53] P. Erätuuli. "Self-resonant antennas in handsets." Master's thesis, Helsinki University of Technology, Espoo, Finland, 1995, p. 56.

[54] P. Haapala. "Dual frequency helical antennas." Master's thesis, Helsinki University of Technology, Espoo, Finland, 1995, p. 51.

[55] Homepage of Schwarzbeck Mess - Elektronik. Internet: `http://www.schwarzbeck.de/Bilder/BBHA9120A.jpg`, [Aug. 26, 2011].

[56] "SCHWARZBECK MESS - ELEKTRONIK, BBHA 9120 A double ridged broadband horn antenna 0.8 – 9 GHz." Internet: `http://www.schwarzbeck.de/Datenblatt/ri9120a.pdf`, [Aug. 26, 2011].

[57] W.L. Stutzman and G.A. Thiele. *Antenna theory and design, 2nd ed..* USA, John Wiley & Sons, 1998, p. 61.